

**The Chulitna Terrane of south-central Alaska: A rifted volcanic arc caught between  
the Wrangellia Composite Terrane and the Mesozoic margin of North America**

Tony Gilman  
Maureen Feineman  
Donald Fisher  
Department of Geosciences  
Pennsylvania State University  
University Park, PA 16802

**Abstract.** Geologic mapping and geochemical analyses of Triassic strata from the Chulitna terrane in south-central Alaska indicate Triassic rifting of a volcanic arc, with development of an asymmetric basin that was later deformed in the Cretaceous within the broadly defined suture between the Wrangellia Composite Terrane and the Mesozoic margin of North America. The structure of the region consists of an overturned synclinorium that verges southeast, with Triassic strata in the core of the syncline and basement rocks exposed in the hanging walls of a series of out-of-syncline thrusts on the southeastern, upright limb. The basement of the complex consists of serpentinite, vesicular flows of basaltic andesite with minor pillow lavas, and volcanic debris with blocks of andesite and minor Devonian red chert. From southeast to northwest, there are systematic changes in the facies associated with Triassic strata that overlie this basement. To the southeast, the basement is unconformably overlain by bedded sedimentary breccias consisting of subangular clasts of basement lithologies, with red chert, serpentinite, and andesite. Further to the northwest, in the hanging wall of a more

rearward thrust, the red bed strata consist of conglomerate intermixed with siltstone and cross-bedded sandstone. In the northwest on the overturned limb of the syncline, the red beds are composed of siltstone and sandstone interfingered with limestone. There is an overall increase in the thickness of the red bed unit from southeast to northwest. On the northwestern limb of the syncline, the red beds overlie a 1500-m-thick basalt sequence with columnar jointed flows and pillow basalts interbedded with limestone. Geochemical analyses of clinopyroxene phenocrysts in the basalts show similarities with island arc basalts, suggesting that volcanism is related to early rifting of an oceanic arc. A marine sandstone unit overlies the entire redbed package along a flooding surface and thins to the southeast. These results are consistent with Triassic deposition within a rifted volcanic arc, with an upland erosion surface to the southeast and increasing thickness of the Triassic section toward a basin-bounding fault in the northwest. This basin was initially approximately 18 km wide prior to accretion along the Mesozoic margin of North America, which resulted in southeast-vergent folding and 30% shortening.

## **Introduction**

Tectonic reconstructions of the northwestern Cordillera are complicated by the collision of arcs and oceanic plateaus as well as subsequent truncation and modification of the margin by Tertiary strike-slip faults. Consequently, the development of tectonic models that integrate patterns of erosion, deformation, metamorphism and sedimentation is limited by the need for paleolatitude, timing, and kinematic constraints on mountain-building events that are in many cases obscured by later deformation. The need for such constraints is particularly apparent in south-central Alaska where the tectonic history is

dominated by the collision of the Wrangellia Composite Terrane (WCT, an amalgamation of the Peninsular, Wrangellia, and Alexander terranes) with the Mesozoic margin of North America (Figure 1). The suture zone of this collision is broadly defined by a belt of marine clastic sedimentary rocks, the Kahiltna assemblage, as well as a number of smaller terranes such as the Chuliltna, West Fork, and Broad Pass terranes (Nokleberg et al., 1994) (Figure 2).

Detailed analyses have illustrated the complexity of the structural and stratigraphic framework of the suture zone of the North America/WCT collision (e.g., Trop and Ridgway, 2007). The thrust sense and fold vergence varies across the region (Csejtey et al., 1992) and locally varies through time (Beam and Fisher, 1999).

Importantly, the Kahiltna assemblage in the Broad Pass area (Figure 2) consists of at least two distinct basins (Ridgway et al., 2002): 1) a northern Talkeetna backarc basin that is Kimmeridgian to Velanginian and consists of northwest-facing fans of sediment derived from the WCT and 2) an Alaska Range oceanic basin that is Velanginian–Cenomanian and consists of southward directed sediment fans with sediment derived from the terranes that make up the Mesozoic margin of North America. Thus, the region between the Talkeetna and Alaska basins marks the boundary between rocks of N. American and WCT affinity.

One of the more enigmatic features of the suture zone of south-central Alaska is the Chuliltna terrane, a fault-bounded sliver of serpentinite, volcanic rocks, red beds, and limestone that lies between the Talkeetna and Alaska Range basins (Figure 2). Jones et al. (1980) described the Chuliltna as unlike any other sequence in Alaska, whereas Clautice et al. (2001) emphasized the similarities to parts of the WCT, given the existence

of a mid-Paleozoic volcanic arc and a thick package of Triassic basalt with interbedded limestones. Much of the debate centers on the origin of these basalts. Moreover, the basement of the Chulitna terrane has been referred to as either an ophiolite based on the occurrence of serpentinite, pillow basalts, and chert or as an oceanic arc based on tholeiitic trend of basaltic andesites (Clautice et al., 2001). Red beds within the terrane have been cited as typical of Triassic deposition at lower latitudes (Jones et al., 1980) or atypical of continental red beds (Clautice et al., 2001), though similar aged red beds occur in the Alexander terrane (Butler et al., 1997). The occurrence of tropical fauna in limestones of the Chulitna suggests large latitudinal displacement in the Mesozoic and an exotic origin with respect to the Mesozoic margin of North America (Nokleberg et al., 1994).

In this paper, we present the results of detailed mapping and structural analysis within the southeastern Chulitna terrane. These observations, combined with geochemical analysis of pyroxenes from Triassic basalts, are used to evaluate the architecture and pre-shortening geometry, the significance of the red beds, and the origin of Triassic volcanism within the Chulitna terrane.

### **Geology of South-central Alaska**

The geology of south-central Alaska can be divided into four distinct terrane groups based on location and timing of accretion (Nokleberg et al., 1994) (Figure 1). These four groups are: (1) terranes amalgamated and accreted to the margin of North America prior to the Mesozoic, (i.e., the Yukon Composite Terrane (YCT)), (2) terranes that make up the Wrangellia composite terrane (WCT), (3) terranes of the Alaska Range

suture zone, including the Chulitna terrane. and (4) accretionary terranes on the south side of the WCT.

The south-facing margin of the Yukon Composite Terrane represents the accretionary backstop against which all of the terranes of southern Alaska accreted in the late Jurassic-Cretaceous. Along part of this margin, these Paleozoic metamorphosed continental margin strata and Mesozoic arc rocks of the YCT are exhumed and deformed into an anticline at 115-106 Ma (Ridgway et al., 2002). The Denali fault, a major North American tectonic boundary with 100's of kms of displacement since the late Cretaceous (Nokleberg et al., 1994; Nokleberg and Richter, 2007), separates the highly deformed southern boundary of the YCT from the terranes of the suture zone to the south (Silberling et al., 1994; Nokleberg et al., 1994; Ridgway et al., 2002).

The Wrangellia Composite terrane (WCT) includes the Wrangellia, Peninsular, and Alexander terranes (Figure 1). The Wrangellia terrane consists of a late Paleozoic sequence of island arc volcanics and related sedimentary rocks overlain by 1500-4000 m of massive basalt flows of the late Triassic Nikolai greenstone locally capped by limestone (Nokleberg et al., 1985; Plafker et al., 1989). Paleomagnetic inclinations for Triassic basalts indicate a near-equatorial position for Wrangellia in the Triassic (Hillhouse and Gromme, 1984), but a moderate paleolatitude and by the late Cretaceous (Stamatakis et al., 2001). Wrangellia was deeply exhumed and proximal to North America by the early Cretaceous (Trop and Ridgway, 2007). There is a 1st order crustal discontinuity along the steeply west-dipping Talkeetna suture zone that separates transitional crust of collisional basins to the north from the thicker interior of the

Wrangellia terrane that may have thickened by magmatic underplating in the Triassic (Glen et al., 2007).

The Peninsular terrane is composed of a variety of tectonostratigraphic units that together define the Talkeetna arc, including Triassic volcanics, limestones, and volcanoclastics, a Late Triassic ultramafic suite, and Middle Jurassic plutonic rocks (Figure 1). The complex was later intruded by Late Cretaceous-Tertiary plutons of the Alaska-Aleutian Ranges Batholith (Plafker et al., 1989). The Alexander Terrane includes a basement of Proterozoic arc-related rocks deformed and metamorphosed in the late Cambrian-early Ordovician, Silurian arc-type volcanics metamorphosed during Late Silurian-early Devonian, with intrusion of trondjemite plutons in the south and northward advance of a clastic wedge (Gehrels et al., 1996). This basement is overlain by upper Triassic clastic sedimentary rocks that include red beds consisting of conglomerates, sandstones and siltstones, with clasts derived from the basement (Gehrels et al., 1996). Zircons from the Triassic rocks give U-Pb ages of 405-440 Ma, indicating an intraterrane source, although 1-3 Ga ages for zircons in a Lower Devonian sandstone suggest proximity to a continent at that time (Gehrels et al., 1996). Volcanic and plutonic stitching, faunal similarities of Permian carbonates, and similar Late Triassic volcanics link these three terranes since the Late Paleozoic (Gehrels and Saleeby, 1987; Gardner et al., 1988). The closure of the suture zone between the YCT and the WCT occurs some time in the late Cretaceous (Ridgway et al., 2002), with a 74 Ma U-Pb age for a large dioritic syntectonic intrusion within the MacLaren metamorphic belt (Davidson et al., 1992).

This study is focused on the Chulitna terrane, a fault-bounded lenticular package of strata approximately 12 km wide by 30 km long located on the north side of the Chulitna River valley in south-central Alaska (Figure 2). The relationship between the Chulitna and other terranes that make up the WCT and YCT in south-central Alaska remains hotly debated. Tropical fauna from Triassic strata of the Chulitna terrane are consistent with an origin exotic to North America (Nokleberg et al., 1994) and suggest an affinity with the WCT. The existence of a Paleozoic arc with a thick sequence of late Triassic tholeiitic basalt shows a similarity to the stratigraphy of Wrangellia (Clautice et al., 2002). However, the existence of a Triassic red bed sequence overlying basement along an unconformity is also observed in the Alexander terrane (Gehrels et al., 1996). Moreover, gastropod fauna from Norian strata in the Chulitna terrane are more similar to those of the Alexander terrane than to Wrangellia (Blodgett et al., 2001). Triassic red beds from the Chulitna terrane contain zircons with mid Paleozoic and Proterozoic U-Pb ages (Hampton et al., 2005), much like the Devonian-Triassic strata of the Alexander terrane (Gehrels et al., 1996). Triassic reef fauna from the Chulitna terrane are well known from Tethyan Triassic reef deposits and are more similar to the Stikine and Eastern Klamath terranes than either Wrangellia or the Alexander terrane (Yarnell and Stanley, 2000). Thus, the paleogeographic and tectonostratigraphic origins of the Chulitna terrane remain in doubt, and much of the debate centers on the origins of the basalts and related Triassic sedimentary rocks.

In this paper, we present the results of geologic mapping and structural analyses in a region near the southwest end of the Chulitna terrane (Figure 3). The Chulitna terrane is bounded to the northwest by the Kahiltna assemblage of the Alaska Range

basin and on the southeast by the West Fork Terrane, the Broad Pass terrane, and the North Talkeetna Mountains basin (Figure 2). The West Fork Terrane in the field area consists of a massive tuff facies and a Late Jurassic argillite-chert facies in thrust fault contact with the Chulitna terrane along the south vergent, northwest dipping Chulitna thrust fault (Jones et al., 1980).

There are four main stratigraphic units exposed within the Chulitna Terrane (Figures 2 and 3): 1) a basement of volcanic flows, volcanoclastics, and serpentinite (Dv), 2) basalts intercalated with limestone (Trlb), 3) red beds (Trrb), and 4) a brownish marine sandstone with lenses of limestone (JTRs). The basement rocks (Dv) consist of vesicular olive green to dark gray basaltic andesites, poorly sorted mixtures of volcanic blocks of chert with Devonian radiolaria (Jones et al., 1980), and serpentinite slivers. The abundant vesicular or amygdaloidal lavas weather tan to white, and grain size varies from very fine to fine-grained. The amygdules range in size from 1 – 5 mm, and are infilled with calcite (Figure 4). The basement in the study area also includes poorly sorted volcanic debris deposits, with clasts ranging in size from tens of centimeters to millimeters. These angular blocks are composed of chert and basaltic andesite in a finer-grained matrix (Figure 5). Serpentinite is exposed in northeast trending slivers that extend along strike. The light to dark green serpentinite weathers to light brown and is typically sheared and altered to magnesite and quartz, with numerous quartz veins and quartz-filled vugs in the vicinity of mapped faults.

In the northwest portion of the map area, the oldest exposed unit is a 1500-m-thick Triassic limestone and basalt (TRlb) sequence that unconformably overlies the basement in the western edge of the map area. Basalts vary from massive, to pillowed, to

columnar (Figure 6a and b), to matrix-supported basalt breccias. The phenocryst assemblage is composed primarily of diopsidic clinopyroxenes 0.5-2 mm diameter, often in clusters, with rare hornblende (commonly replaced by biotite and/or oxides) up to 3 mm diameter, and smaller (~100  $\mu\text{m}$ ) matrix plagioclase (Figure 7). Secondary minerals include micas, chlorite, oxides, and calcite. The basalt is dark gray to black and weathers orange to tan. The limestone within this unit is fossiliferous, weakly metamorphosed wackestone to packstone, with minor grainstone observed immediately below the contact with the Triassic redbed. It is light gray to gray in color and thickly bedded.

The Triassic redbeds (TRrb) vary in facies from southeast to northwest with three distinct outcrop belts. These belts are: (1) a red massive to thick-bedded sedimentary breccia that unconformably overlies the basement (Figure 8a and 8b), (2) a red, more thinly bedded sequence that includes conglomerate, arkosic sandstone, and siltstone (Figure 9), and (3) arkosic sandstone and siltstone interbedded with limestone (Figure 10). In the southeastern part of the area, the redbed breccia is approximately 250-500 m thick with grain size that varies from millimeters to tens of centimeters. The grains are extremely angular and moderately sorted, with clasts primarily composed of the underlying red radiolarian chert, with lesser amounts of basaltic andesite, and serpentinite of the Devonian basement with a carbonate cement. The redbed breccia is weakly bedded with beds ranging in thickness from 0.5-2.0 m. The redbeds lie unconformably over the Devonian basement along a planar unconformity.

Further to the northwest, the redbed unit is composed of conglomerate with cross-bedded sandstone and siltstone (Figure 9). The unit ranges in thickness from 500-750 m. The grains within the conglomerate vary from millimeter to centimeter-size, semi-angular

to semi-rounded, and are well sorted. Bedding thicknesses vary from 15 - 80 cm, with the clasts composed of radiolarian chert, basalt, and serpentinite of the Devonian basement. The redbed in the central portion of the terrane lies unconformably on the Devonian basement rocks and conformably underlies the Jurassic-Triassic brown sandstone.

In the northwestern-most portion of the study area, the Triassic redbeds are composed of sandstone and siltstone interbedded with marine limestone (Figure 10). The redbed is approximately 0.75 - 1 km thick in this portion of the terrane. The grains are semi-rounded to rounded, well sorted, and very fine grained to medium grained. The beds range in thickness from 5-50 cm, and occasionally display cross-beds. The unit is red and white and weathers gray to brown. The redbed unit in this part of the field area is in conformable contact above and below with the Jurassic-Triassic brown sandstone and Triassic limestone and basalt unit, respectively.

The youngest unit within the Chulitna terrane is a marine Triassic-Jurassic brown calcareous sandstone and argillite unit exposed in the belt that forms the core of a syncline within the center of the study area. This assemblage increases in thickness to the northwest. The unit is thickly bedded with bedding varying from 10-30 cm. Fossils are abundant in the lower portion of the unit and consist of corals, bivalves, and the distinctive Late Triassic-Early Jurassic spherical hydrozoans. The sandstone and argillite unit is brown to gray, weathers orange to tan, and contains no visible sedimentary structures. Petrographic analysis of the brown sandstone and argillite unit displays very angular clasts in a calcite matrix. The unit thins from the northwest to the southeast.

## Geochemistry of the Triassic Basalts

Major element analysis of clinopyroxenes (Table 1) was performed using the Cameca SX-50 electron microprobe operated by the Materials Characterization Laboratory (MCL) at Pennsylvania State University. Analyses were performed using an accelerating voltage of 15kV and a beam current of 12 nA. The beam diameter was 10 mm. Observed X-ray intensities in the unknown samples were converted to weight concentrations of analyte elements using measured intensities on synthetic and natural mineral standards and corrected for matrix effects using a PAP (phi-rho-Z) method (Pouchou and Pichou, 1987). Major element concentrations are reported as weight % oxides.

Trace elements were analyzed by laser ablation inductively coupled plasma mass spectrometry (LA-ICP-MS) (Table 2) using the Finnigan Element I magnetic sector ICP-MS and New Wave UP213 Nd:YAG deep UV (213nm) laser operated by the Materials Characterization Laboratory (MCL) at Pennsylvania State University. Samples were analyzed at a 10 Hz repeat rate, 45% of maximum beam energy, and a spot size of ~85  $\mu\text{m}$  diameter. A combined Ar and He carrier gas was used to maximize sampling efficiency.

Trace element concentrations (Table 2) were obtained by comparing  $^{43}\text{Ca}$  - normalized count rates for the unknown samples to  $^{43}\text{Ca}$ -normalized count rates from synthetic glass standards (NIST-612, BHVO-2g, and BCR-2g). Data were collected in batches of 5-10 analyses bracketed on both sides by standard analyses. Isotopes measured were  $^{43}\text{Ca}$ ,  $^{47}\text{Ti}$ ,  $^{49}\text{Ti}$ ,  $^{85}\text{Rb}$ ,  $^{86}\text{Sr}$ ,  $^{89}\text{Y}$ ,  $^{90}\text{Zr}$ ,  $^{93}\text{Nb}$ ,  $^{133}\text{Cs}$ ,  $^{137}\text{Ba}$ ,  $^{139}\text{La}$ ,  $^{140}\text{Ce}$ ,  $^{146}\text{Nd}$ ,  $^{147}\text{Sm}$ ,  $^{151}\text{Eu}$ ,  $^{172}\text{Yb}$ ,  $^{175}\text{Lu}$ ,  $^{178}\text{Hf}$ , and  $^{181}\text{Ta}$ . The trace elements Rb, Nb, Cs, Ba, and Ta

were below detection limits in most samples and are not discussed further. Replicate analyses of standard glasses (BHVO-2g and BCR-2g) yield a relative standard deviation of <10%, and deviation from published values is better than 10% for most elements.

Clinopyroxenes in altered basalts are of interest because they often survive in relatively pristine form after the matrix and other minerals have been converted to secondary minerals. The major and minor element geochemistry of clinopyroxenes is varied and provides a filtered view of the composition of the magma from which the clinopyroxene crystallized, lending it the potential to provide insight into the tectonic origins of altered basalts (Nisbet and Pearce, 1977; Letterier et al., 1982; Beccaluva et al., 1989). The preserved clinopyroxenes in the altered Chulitna Triassic basalts are diopsidic, with rims slightly enriched in Fe relative to the cores (Figure 11). This type of normal zoning is typical of magmatic clinopyroxenes, and does not provide unique insight into the origins of this basalt. However, several discrimination diagrams have been developed based on major and minor element variations in clinopyroxene that allow us to assess the nature of these rocks, with the goal of determining the tectonic environment of the Chulitna terrane at the time that the basalts were formed.

A series of simple discrimination diagrams was devised by Letterier et al. (1982) in order to distinguish the origins of paleobasalts based on clinopyroxene compositions. Three separate diagrams were developed to distinguish alkalic from sub-alkalic basalts (Ca+Na vs. Ti), orogenic from non-orogenic basalts (Ca vs. Ti+Cr), and calcalkaline orogenic basalts from tholeiitic orogenic basalts (Al vs. Ti). On the basis of these diagrams (Figure 12), we can see that the Chulitna basalts are clearly sub-alkaline. They are dominantly orogenic in nature, although the clinopyroxene compositions do have a tail

that extends into the non-orogenic field, which is a common feature of basalts formed in rifted arcs. The clinopyroxenes with orogenic compositions lie definitively in the tholeiitic field. To summarize, the Chulitna basalts appear to be tholeiitic basalts with a strong orogenic flavor, but with a clear extension into the non-orogenic compositional domain.

Another method for distinguishing basalt compositions based on clinopyroxene compositions adds another dimension by plotting  $\text{TiO}_2$ ,  $\text{SiO}_2/100$ , and  $\text{Na}_2\text{O}$  on a ternary diagram (Beccaluva et al., 1989). Similar to the Letterier et al. discrimination plots, this diagram exploits the difference in fluid-immobile incompatible element (i.e.  $\text{TiO}_2$ ) concentrations between different basalt types. As can be seen in Figure 13, there is a lot of overlap between basalt types on this diagram. Most of the Chulitna clinopyroxene compositions lie within the arc tholeiite field, consistent with the results determined by application of the Letterier et al. diagrams. We have added a field to this plot to show the location of clinopyroxenes from a back-arc basalt (Lau Basin, data from Bryan et al., 1994). The overlap between the arc tholeiite and back-arc basalt fields is such that all but a few  $\text{TiO}_2$ -poor clinopyroxenes from Chulitna are also consistent with a back-arc basalt origin.

Perhaps the most definitive categorical separation of basalt types according to clinopyroxene composition is the initial work of Nisbet and Pearce (1977). The authors use statistical analysis of clinopyroxene compositions to determine discriminant functions for distinguishing basalt types. Figure 14 shows a ternary plot of  $\text{TiO}_2$ ,  $\text{MnO}$ , and  $\text{Na}_2\text{O}$  in clinopyroxene. These oxide concentrations correspond to the three discriminant

functions determined by Nisbet and Pearce. Plotting the clinopyroxene compositions for the Chulitna basalts on this diagram suggests that these basalts are unlikely to be within-plate basalts. Based on Nisbet and Pearce's differentiation scheme, the clinopyroxene compositions are again most consistent with a volcanic arc origin, although limited compositional extension into another basalt field is possible.

Geochemical analyses of the Triassic basalts also hold clues to their tectonic origin because the trace element composition of a basalt reflects the mantle sources and processes that came together to produce it. This includes the relative degree of depletion of the mantle, the melt fraction, elemental fractionation by residual phases as determined by their pressure-dependent stabilities, and metasomatic effects due to the infiltration of externally derived fluids prior to melting. Due to the broad variation in these combined factors, basalts produced in different tectonic settings have different characteristic trace element compositions. For example, island arc basalts (IAB) are typically enriched in fluid mobile elements relative to mid-ocean ridge basalts (MORB) due to metasomatism of the mantle wedge by fluids derived from the subducting slab. Back-arc basin basalts (BABB) are typically intermediate between IAB and MORB, reflecting their origins in shallow extensional regions of the mantle, similar to the MORB-source region, but containing a small contribution from subduction zone fluids.

Equilibrium melt compositions for the Chulitna basalts have been calculated by applying published clinopyroxene/melt partition coefficients (Sobolev et al., 1996) to our measured clinopyroxene trace element compositions. The calculated melt compositions normalized to MORB are plotted in Figure 15. The most obvious feature observed by plotting the data in this way is the clear difference between the “low Zr” and “high Zr”

samples (labeled Melt “A” and Melt “B”, respectively). Specifically, the high-Zr clinopyroxene data generate a calculated melt composition (Melt B) that is atypically enriched in fluid-immobile elements (i.e. REE, Zr) and relatively depleted in fluid-mobile elements (i.e. Sr). We interpret this pattern to be indicative of post-crystallization alteration of the clinopyroxene, and not indicative of original melt compositions. For this reason, the Melt B data are considered no further. Melt A, by contrast, shows a clear enrichment in Sr and light REE (LREE) relative to MORB. More specifically, Sr is enriched relative to the LREE, and the LREE are enriched relative to the heavy REE (HREE). This pattern of trace element fractionation is characteristic of IAB, as can be seen by comparison to the average IAB composition of McCulloch and Gamble (1991).

### **Structural Geology of the Chulitna Terrane**

The main structure in the Chulitna terrane is a tight synclinorium overturned to the southeast with northwest dipping beds on both limbs (Figure 16a). The southeast upright limb of the synclinorium contains three out-of-syncline thrust faults, two that place the volcanics of the Devonian basement over the Triassic red bed unit, and one that places the serpentinite on top of the volcanics of the basement. The furthest southeast thrust fault at the base of the Devonian volcanics emplaces the Chulitna terrane on the younger West Fork terrane to the southeast along the Chulitna thrust fault of Jones et al. (1980). The Jurassic-Triassic brown marine sandstone makes up the core of the synclinorium and is bracketed on either side by the Triassic redbeds. A pervasive cleavage is restricted to sandstones in the core of the synclinorium. The Triassic

limestone and basalt unit is in depositional contact with the overlying terrestrial redbeds on the northwest overturned limb of the regional synclinorium.

The axial plane of the synclinorium dips approximately 45° toward the northwest. The folding is tight, with kink fold geometry. Smaller second order folds display reversals in vergence across the hinge of the first order syncline, suggesting they are parasitic folds in an area dominated by regional southeast-directed vergence. A  $\pi$ -diagram of all bedding measurements yields a fold axis orientation with a trend of 31.5° and plunge of 35°. The axial planes of the second order folds dip between 25° to 35° to the northwest. The wavelength of the parasitic folds is on the order of hundreds of meters with amplitudes of similar magnitude.

A reconstruction of the geometry of the stratigraphic packages based on the cross section along line A-A' from Figure 3 is shown in Figure 16b. The length of the cross section line is approximately 8 km, whereas the length was likely 12 km or greater prior to shortening associated with folds and thrust faults.

## **Discussion**

The Chulitna terrane displays a variety of characteristics that indicate Triassic rifting of a volcanic arc and development of a fault-bounded rift basin sequence. First, there is a planar unconformity along the southeastern portion of the Chulitna terrane that separates terrestrial gravels of the Triassic redbed unit from the underlying basement. The gravels are angular and composed of basement lithologies suggesting that they are not far-travelled. We interpret the dominance of red chert over other basement lithologies as being due to preferential preservation of competent materials during

transport. Quartz clasts within these beds could easily be derived from quartz veins in the basement rather than requiring a nearby continental source (e.g. Jones et al., 1980). In a classic rift basin assemblage, normal faulting leads to creation of accommodation space and onlap of an unconformity on the non-faulted side of a half-graben (Manspeizer, 1988; Manspeizer et al., 1989; Davis and Reynolds, 1996). The unconformity, in combination with increasing roundness and decreasing grain size within the red bed unit from southeast to northwest, suggests sediment transport from uplands in the southeast toward a marine basin in the northwest.

There are also systematic variations in the total Triassic section above basement, with an increase in thickness of all three of the major Triassic-Jurassic units to the northwest. The basalt-limestone section is absent above the basement erosional unconformity to the southeast but displays an accumulation of 1500 m in shallow marine conditions to the northwest. The red beds double in thickness from 250-500 m overlying the unconformity in the southeast to 750-1200 m on the overturned limb of the syncline to the northwest. The brown marine sandstone also thickens to the northwest. The absence of the marine carbonate facies in the red beds to the southeast and the abundant intercalated marine limestones in the red beds to the northwest are consistent with a northwest-facing shoreline. The variation in sedimentary environments inferred from facies characteristics, coupled with the increasing thickness of stratigraphic units indicates that the creation of accommodation space increases to the northwest across the transect. This pattern is thus consistent with deposition within a rift basin bounded to the northwest by a southeast-facing normal fault that is not directly observed.

Reconstruction of the depositional positions prior to southeast-vergent folding indicates a basin that was approximately 12-20 km wide with marked facies changes from southeast to northwest related to position within a restricted basin. A rift basin origin for the strata of the Chulitna terrane would explain the differences between this stratigraphic section and strata from other parts of the WCT. The brown sandstone unit represents a marine flooding surface that marks the rift to drift transition as is seen along passive continental margins.

On the basis of the major and minor element chemistry of the remnant clinopyroxenes in the Chulitna basalt, as well as the trace element composition of the original melt as inferred from the clinopyroxene compositions, we argue that the Chulitna basalts are island arc basalts or basalts produced during the earliest stages of back-arc rifting, when basalt compositions are still very similar to IAB (e.g. Lau Basin basalts, Kamenetsky et al., 1997). A model that invokes the initiation of back-arc rifting is consistent with evidence that strata were deposited within a rift basin. We find no geochemical indication that these rocks are flood basalts, as would be expected if they were analogous to the Nikolai greenstones of the Wrangellia terrane (Clautice et al., 2001), although this could be a local variant where trace element chemistry is influenced by sub-arc mantle. Based on this model of arc-rifting, we interpret ultramafic slivers and volcanics of the Devonian Chulitna basement as a suprasubduction ophiolite, similar to younger upper Triassic mafic and ultramafic rocks between the WCT and North America in the Lake Clark Region (Amato et al., 2007).

South-vergent folding of the stratigraphic packages that make up the Chulitna terrane likely occurred during the south-directed thrusting in the Late Cretaceous (Trop

and Ridgway, 2007) that typifies the South Alaska Basin (Bier, pers. comm.) and the MacLaren metamorphic belt to the northeast (Davidson et al., 1992). Thus, we interpret this deformation as postdating the oblique initiation of collision in the upper Jurassic to early Cretaceous (Trop and Ridgway, 2007).

## **Conclusions**

We conclude that the Chulitna terrane is an extensional basin related to rifting of a volcanic arc. The terrane has a basement of volcanic rocks and serpentinite that represents the upper plate of an oceanic arc. A regionally extensive unconformity separates basement from a Triassic rift sequence with coarse immature fluvial redbeds in the southeast of the study area and a thick accumulation of basalt and red siltstone interbedded with limestone in the northwest. The greater accommodation space to the northwest indicated by the increasing thickness of stratigraphic packages and the interfingering of marine facies is consistent with an asymmetric basin architecture with a Triassic normal fault to the northwest now obscured by later deformation associated with the docking of the WCT with North America. The major and minor element geochemistry of Triassic basalt suggests an island arc origin that likely reflects the early stages of back-arc rifting. Restoration of collision-related south-east directed folding and thrusting in the study area is consistent with a restricted basin that is elongate to the northeast and 12-20 km wide, with a northeast-trending coastline and large variation in depositional environments from highlands in the southeast toward a linear depocenter in the northwest. Isolated basins around the edge of the WCT such as the Chulitna terrane may have very different stratigraphic records despite similar paleogeographic origins.

- Amato, J. M., Bogar, M. J., Gehrels, G. E., Farmer, G. I., and McIntosh, W. C., 2007, The Tilkakila complex in southern Alaska: a suprasubduction-zone ophiolite between the Wrangellia Composite terrane and North America, *in* Ridgway, K. D., Trop, K. M., Glen, J. M. G., and O'Neill, J. M., eds., *Tectonic Growth of a Collisional Continental Margin: Crustal Evolution of Southern Alaska*: Geological Society of America Special Paper 431, p. 227-252, doi: 10.1130/2007.2431 (10).
- Beccaluva, L., Macciotta, G., Piccardo, G.B., and Zeda, O., 1989, Clinopyroxene composition of ophiolite basalts as petrogenic indicator: *Chemical Geology*, v. 77, p. 165-182.
- Beam, E. and Fisher, D., 1999, Rotation of elongate porphyroblasts in a shear zone, south-central Alaska: *Journal of Structural Geology*, v. 21, no. 11, p. 1553-1559.
- Blodgett, R. B., and Fryda, J., 2001, Upper Triassic gastropod biogeography of western North America: *Geological Society of America Abstract With Program*, v. 33, no. 3, p. 53.
- Bryan, W., Ewart, A., Grove, T., and Pearce, T., 1994, Natural phase equilibria and petrologic models: Lau Basin sites 834, 836, and 839, *in* Hawkins, J., Parson, L., Allan, J., et al., eds., *Proceedings of the Ocean Scientific Drilling Program Scientific Results*, v. 135, p. 487-503.
- Butler, R. F., Gehrels, G. E., and Bazard, D. R., 1997, Paleomagnetism of Paleozoic strata of the Alexander terrane, southeastern Alaska: *Geological Society of America Bulletin*, v. 109, no. 10, p. 1372-1388.
- Clautice, K. H., Newberry, R.J., Blodgett, R. B., Bundtzen, T.K., Gage, B.G., Harris, E.E., Liss, S.A., Miller, M.L., Reifenstuhel, R.R., Clough, J.G., and Pinney, D.S., 2001, Bedrock geologic map of the Chulitna region, Southcentral Alaska: Alaska Division of Geological and Geophysical Surveys, Report of Investigations 1997-14A, scale 1:125, 000.
- Csejtey, B., Jr., Mullen, M. W., Cox, D. P., and Stricker, G. D., 1992, Geology and geochronology of the Healy quadrangle, south-central Alaska: U. S. Geological Survey Miscellaneous Investigation Map I-1961. scale 1:250,000.

- Davidson, C., Hollister, L. S., and Schmid, S. M., 1992, Role of melt in the formation of a deep-crustal compressive shear zone: The MacLaren Glacier metamorphic belt, south-central Alaska: *Tectonics*, v. 11, p. 348-359.
- Davis G.H. and Reynolds, S.J., 1996, *Structural Geology of rocks and regions: Colorado*, John Wiley and Sons, Inc., second edition.
- Gardner, M. C., Bergmann, S. C., MacKevett, E. M., Jr., Plafker, G., Campbell, R. C., Cushing, G. W., Dodds, C. J., and McClelland, W. D., 1988, Middle Pennsylvanian pluton stitching of Wrangellia and the Alexander terrane, Wrangell Mountains, Alaska: *Geology*, v. 16, p. 967-971.
- Gehrels, G. E., Butler, R. F., and Bazard, D. R., 1996, Detrital zircon geochronology of the Alexander terrane, southeastern Alaska, *Geological Society of America Bulletin*, v. 108, no. 6, p. 722-734.
- Gehrels, G. E., and Saleeby, J. B., 1987, Geologic framework, tectonic evolution, and displacement history of the Alexander terrane: *Tectonics*, v. 6, p. 151-173.
- Glen, J. M. G., Schmidt, J., Pellerin, L., McPhee, D. K., O'Neill, J. M., 2007, Crustal structure of Wrangellia and adjacent terranes inferred from geophysical studies along a transect through the northern Talkeetna Mountains, *in* Ridgway, K. D., Trop, K. M., Glen, J. M. G., and O'Neill, J. M., eds., *Tectonic Growth of a Collisional Continental Margin: Crustal Evolution of Southern Alaska*: Geological Society of America Special Paper 431, p. 21-41, doi: 10.1130/2007.2431(02).
- Hampton, B. A., and Ridgway, K. D., and Gehrels, G. E., 2005, Detrital Zircon record of the configuration and evolution of the Alaska Range suture zone, south-central Alaska: *Geological Society of America Abstract With Program*, v. 37, no. 7, p. 81.
- Hillhouse, J. W. and Grommé, C. S., 1984, Northward displacement and accretion of Wrangellia: New paleomagnetic evidence from Alaska, *Journal of Geophysical Research*, v. 89, p. 4461-4467.
- Jones, D. L., Silberling, N.J., Coney, P.J., and Plafker, G., 1987, Lithotectonic terrane map of Alaska (west of the 141st meridian), U.S. Geological Survey Report MF-1874-A.

- Jones, D. L., Silberling, N.J., Csejtey, J.R., Nelson, W.H., and Blome, C.D., 1980, Age and Structural Significance of Ophiolite and Adjoining Rocks in South-central Alaska, U.S. Geological Survey Professional Paper.
- Kamenetsky, V., Crawford, A., Eggins, S., and Muehe, R., 1997, Phenocryst and melt inclusion chemistry of near-axis seamounts, Valu Fa Ridge, Lau Basin: insight into mantle wedge melting and the addition of subduction components: *Earth and Planetary Science Letters*, v. 151, p. 205-223.
- Leterrier, J., Maury, R., Thono, P., Girard, D., and Marchal, M., 1982, Clinopyroxene composition as a method of identification of the magmatic affinities of paleo-volcanic series: *Earth and Planetary Science Letters*, v. 59, p. 139-154.
- Manspeizer, W., 1988, Triassic-Jurassic rifting and opening of the Atlantic: An overview, *in* Manspeizer, W., eds., *Triassic-Jurassic rifting: Amsterdam, Elsevier Scientific Publishers, Developments in Geotectonics*, v. 22, p. 41-80.
- Manspeizer, W., DeBoer, J., Costain, J.K., Froelich, A.J., Coruh, C., Olsen, P.E., McHone, G.J., Puffer, J.H., and Prowell, D.C., 1989, Post-Paleozoic activity, *in* Hatcher, R.D., Jr., Thomas, W.A., and Viele, G.W., eds., *The Appalachian-Ouchita Orogen in the United States: Boulder, Colorado, Geological Society of America, The Geology of North America*, v. F-2, p. 319-373.
- McCulloch, M., Gamble, J., 1991, Geochemical and geodynamical constraints on subduction zone magmatism: *Earth and Planetary Science Letters*, v. 102, p. 358-374.
- Monger, J.W.H. and Berg, H.C., 1987, Lithotectonic terrane map of Western Canada and southeastern Alaska, U.S. Geological Survey Report MF-1874-B.
- Nisbet, E. and Pearce, J., 1977, Clinopyroxene composition in mafic lavas from different tectonic settings: *Contributions to Mineralogy and Petrology* v. 63, p. 149-160.
- Nokleberg, W. J., Jones, D. L., and Silberling, N. J., 1985, Origin and tectonic evolution of the Maclaren and Wrangellia terranes, eastern Alaska Range, Alaska, *Geological Society of America Bulletin*, v. 96, p. 1251-1270.
- Nokleberg, W.J., Plafker, G., and Wilson, F.H., 1994, Geology of south-central Alaska, *in* Plafker, G. and Berg, H.C., eds., *The Geology of Alaska: Boulder, Colorado, Geological Society of America, The Geology of North America*, v. G-1, p. 311-365.

- Nokleberg, W. J., and Richter, D. H., 2007, Origin of narrow terranes and adjacent major terranes occurring along the Denali fault in the Eastern and Central Alaska Range, *in* Ridgway, K. D., Trop, K. M., Glen, J. M. G., and O'Neill, J. M., eds., Tectonic Growth of a Collisional Continental Margin: Crustal Evolution of Southern Alaska: Geological Society of America Special Paper 431, p. 129-154, doi: 10.1130/2007.2431(06).
- Plafker, G., Nokleberg, W. J., Lull, J. S., 1989, Bedrock geology and tectonic evolution of the Wrangellia, Peninsular, and Chugach terranes along the Trans-Alaska Crustal Transect in the Chugach Mountains and southern Copper River basin, Alaska *in* Page, R. A. (ed.) Special section on northern Chugach Mountains-southern Copper River basin segment of the Alaskan Transect; Part 1 [modified]: *Journal of Geophysical Research*, v. 94, p. 4255-4295.
- Pouchou, J. and Pichou, F., 1987, Basic expression of "PAP" computation for quantitative EPMA, *in* Brown, J.D and Packwood R.H., eds., International Congress, 11th: X-Ray Optics and Microanalysis, Ontario Univ. Press, p. 249–252.
- Ridgway, K. D., Trop, J. M., Nokleberg, W. J., Davidson, C. M., and Eastham, K. R., 2002, Mesozoic and Cenozoic tectonics of the eastern and central Alaska Range: Progressive basin development and deformation in a suture zone: *Geological Society of America Bulletin*, v. 114, p. 1480-1504.
- Silberling, N.J., Jones, D.L., Monger, J.W.H., Coney, P.J., Berg, H.C., and Plafker, George, 1994, Lithotectonic terrane map of Alaska and adjacent parts of Canada: *in* Plafker, George, and Berg, H.C., eds., *The Geology of Alaska: The Geology of North America*, v. G-1, Geological Society of America DNAG Series, 1 sheet, scale 1:2,500,000.
- Stamatakis, J., Trop, J., and Ridgway, K., 2001, Late Cretaceous paleogeography of Wrangellia; paleomagnetism of the MacColl Ridge Formation, southern Alaska, revisited: *Geology*, v. 29, p. 947-950.
- Sun, S.-S., McDonough, W., 1989, Chemical and isotopic systematics of oceanic basalts: implications for mantle composition and processes, *in* Saunders, A. and Norry, M., eds., *Magmatism in the Ocean Basins: Geological Society Special Publication* v. 42, p. 313-345.

- Trop, J. M., and Ridgway, K. D., 2007, Mesozoic and Cenozoic tectonic growth of southern Alaska: a sedimentary perspective, *in* Ridgway, K. D., Trop, K. M., Glen, J. M. G., and O'Neill, J. M., eds., *Tectonic Growth of a Collisional Continental Margin: Crustal Evolution of Southern Alaska: Geological Society of America Special Paper 431*, p. 55-94, doi: 10.1130/2007.2431(04).
- Wallace, W. K., Hanks, C. L., and Rogers, J. F., 1989, The southern Kahiltna terrane: Implications for the tectonic evolution of southwestern Alaska: *Geological Society of America Bulletin*, v. 101, p. 1389-1407.
- Yarnell, J. M., and Stanley, G., 2000, Two Triassic reef faunas from terranes in Alaska and Yukon and their paleogeographic significance, *Geol. Soc. Am. Abstr. With Prog.* v. 32, no. 7, p. 12.

Figure 1. Simplified terrane map of Alaska, modified from Jones et al. (1987), Monger and Berg (1987), and Silberling et al. (1994). The legend and interpretations are modified from Wallace et al. (1989).

Figure 2. Simplified regional terrane map of south central Alaska, modified from Jones et al. (1987), Monger and Berg (1987), and Silberling et al. (1994). The Chulitna terrane is located on the boundary between the southern Alaska Range Kahiltna basin to the north and the northern Talkeetna Mountains Kahiltna basin to the south. Box shows the location of geologic map in Figure 3.

Figure 3. Geologic map of the southwestern Chulitna terrane. The study area lies within the Healy A-6, 1:63,360 United States Geologic Survey quadrangle. Mapping was completed on 1:24,000 topographic base maps.

Figure 4. Sample of amygduloidal basaltic andesite of the early Paleozoic basement of the Chulitna terrane.

Figure 5. Volcanic debris flow of the early Paleozoic basement of the Chulitna Terrane.

Figure 6. a) Columnar-jointed Triassic basalts on the steep to overturned limb of the regional synclinorium. b) Triassic pillow basalts.

Figure 7. Photomicrograph of a clinopyroxene phenocryst in Triassic basalt.

Figure 8. a) Photo of unconformity between the red beds (Trb) and the basement (Dv) on the upright limb of the regional synclinorium along the drainage basin of Little Shotgun Creek. Section is repeated along out-of-syncline thrust. b) Layered sedimentary breccia of the red beds overlying the unconformity.

Figure 9. Cross-bedded sandstones and siltstone of the Triassic red bed unit.

Figure 10. Overturned limb of the regional synclinorium along the northwest edge of the study area. Light-colored layers are interbedded limestones.

Figure 11. Clinopyroxene major element compositions. Molar proportions of wollastonite, enstatite, and ferrosilite in phenocrysts from the Chulitna basalt are plotted on a conventional clinopyroxene ternary diagram. The Chulitna cpx is diopsidic, with slight iron enrichment in the rims relative to the cores.

Figure 12. Clinopyroxene discrimination diagrams after Letterier et al. 1982. a) Plot of Ca+Na vs. Ti indicates that the Chulitna basalts are sub-alkaline. b) Plot of Ca vs. Ti+Cr suggests that the Chulitna basalts span the range from orogenic to non-orogenic composition. Clinopyroxene compositions from Lau Basin basalts (Bryan et al. 1994) are shown as small spots for comparison. The Lau Basin basalts, which sample a freshly rifted arc, also vary continuously from the orogenic to non-orogenic domains. c) Plot of Al vs. Ti indicates that the Chulitna basalts are tholeiites. Only the cpx crystals identified as orogenic on the Ca vs. Ti+Cr diagram are plotted. All data in plots a, b, and c are given in cation proportions.

Figure 13. Clinopyroxene discrimination diagram after Beccaluva et al. 1989. Ternary plot of TiO<sub>2</sub>, SiO<sub>2</sub>/100, and Na<sub>2</sub>O, showing characteristic ranges of cpx compositions from different tectonic settings. OIB = ocean island basalt; MORB = mid-ocean ridge basalt; BABB = back-arc basin basalt. Fields are from Beccaluva et al. 1989, except for BABB, which is based on data for the Lau Basin from Bryan et al. 1994. All data are in oxide weight percents. Our data fall

almost entirely within the arc tholeiite field, although they would also be consistent with origin in a back-arc basin.

Figure 14. Clinopyroxene discrimination diagram after Nisbet and Pearce, 1977.

Ternary plot of  $\text{TiO}_2$ ,  $\text{MnO}$ , and  $\text{Na}_2\text{O}$ , showing characteristic ranges of cpx compositions from different tectonic settings. MORB = mid-ocean ridge basalts; AFB = alkali flood basalts; TFB = tholeiitic flood basalts; IAB = island arc basalts, ALL = compositional overlap zone for cpx in basalts from any tectonic region. All data are in oxide weight percents. Our results are most consistent with an island arc origin.

Figure 15. Model basalt trace element compositions. Trace element compositions in clinopyroxene crystals have been converted to basalt liquid compositions using equilibrium partition coefficients, and are then normalized to MORB. Shown for comparison are average IAB data from McCulloch and Gamble 1991, average OIB data from Sun and McDonough 1989, and Lau Basin BABB data from Kamenetsky et al 1997. MORB normalization values are from Sun and McDonough 1989. The trace element compositions of cpx grains from the Chulitna Triassic basalts fall into two groups, a low-Zr group and a high-Zr group (see Table B), and these compositional differences are apparent in the model basalt melts (called "A" and "B", respectively). The group A (low-Zr) basalts have trace element fractionation patterns similar to average island arc basalt. The group B (high-Zr) basalts do not resemble any average basalt, and are believed to reflect post-crystallization alteration of the clinopyroxene.

Figure 16. a) Cross section along line A-A' in Figure 3. No vertical exaggeration. Scale bar in meters. b) Reconstruction based on preservation of line length along the unconformity and preservation of area for Triassic units between the deformed and undeformed states. Minimum shortening related to subsurface due to the absence of hangingwall cutoffs along the out-of-syncline thrust on the upright limb of the syncline.

**Table 1. Major element concentrations in clinopyroxene**

	cpx1 core	2 $\sigma$ n = 3	cpx1 rim	2 $\sigma$ n = 2	cpx2 core	2 $\sigma$ n = 3	cpx2 rim	2 $\sigma$ n = 3	cpx3 core	2 $\sigma$ n = 2
SiO <sub>2</sub>	53.60	1.92	53.52	0.17	54.02	0.75	53.50	1.34	52.16	1.28
TiO <sub>2</sub>	0.21	0.09	0.15	0.07	0.24	0.09	0.22	0.13	0.29	0.16
Al <sub>2</sub> O <sub>3</sub>	0.90	0.20	0.60	0.30	1.05	0.69	1.04	0.43	0.97	0.18
Cr <sub>2</sub> O <sub>3</sub>	0.31	0.22	0.23	0.10	0.49	0.18	0.37	0.20	0.27	0.27
FeO*	6.34	6.99	8.17	1.02	4.54	1.33	6.25	6.73	4.98	2.14
MnO	0.20	0.23	0.31	0.12	0.20	0.05	0.19	0.21	0.15	0.08
MgO	15.66	5.12	14.13	0.36	16.40	0.96	15.03	4.63	16.55	0.96
CaO	22.06	0.46	22.66	0.25	22.59	0.73	22.16	0.65	22.41	1.09
Na <sub>2</sub> O	0.19	0.08	0.16	0.02	0.21	0.15	0.21	0.00	0.21	0.08
K <sub>2</sub> O	0.00	0.01	0.02	0.01	0.01	0.01	0.00	0.00	0.00	0.00
Total	99.49		99.94		99.73		98.98		97.98	
Wo	45.06	1.82	46.29	0.64	45.98	0.89	46.04	0.38	45.33	1.56
En	44.45	13.54	40.17	1.13	46.47	2.77	43.39	12.05	46.58	2.05
Fs	10.50	11.83	13.55	1.77	7.55	2.18	10.57	11.78	8.08	3.61

	cpx5 core	2 $\sigma$ n = 3	cpx5 rim	2 $\sigma$ n = 3	cpx6 core	cpx6 rim	cpx7 core	cpx7 rim
SiO <sub>2</sub>	53.59	2.75	52.99	0.99	51.0	52.0	52.13	50.99
TiO <sub>2</sub>	0.35	0.57	0.48	0.27	1.0	0.3	0.68	0.91
Al <sub>2</sub> O <sub>3</sub>	1.78	1.92	1.89	0.88	3.4	1.1	2.49	3.00
Cr <sub>2</sub> O <sub>3</sub>	0.60	0.47	0.68	0.07	0.5	0.0	0.25	0.26
FeO*	5.21	3.16	7.00	0.91	8.5	12.5	9.48	9.89
MnO	0.18	0.03	0.26	0.09	0.2	0.4	0.32	0.34
MgO	16.27	2.93	15.10	0.79	13.3	11.6	13.73	13.00
CaO	21.62	0.70	21.49	0.37	21.2	20.2	20.87	20.96
Na <sub>2</sub> O	0.24	0.03	0.24	0.03	0.3	0.2	0.22	0.26
K <sub>2</sub> O	0.01	0.02	0.01	0.02	0.0	0.1	0.01	0.01
Total	99.86		100.1		99.4	98.5	100.1	99.62
Wo	44.60	0.94	44.59	0.24	45.6	43.4	43.81	44.56
En	46.64	6.24	43.61	1.64	39.8	34.8	40.10	38.45
Fs	8.75	5.57	11.80	1.67	14.60	21.83	16.09	16.99

Major element data collected using the Cameca XS-50 electron microprobe at Pennsylvania State University

**Table 2. Trace element concentrations in clinopyroxene**

<i>low-Zr cpx</i>											
	cpx-a	cpx-b	cpx-d	cpx-e	cpx-f	cpx-h	cpx-i	cpx-l	cpx-m	cpx-n	cpx-o
Sr	57.6	59.4	73.7	75.6	72.0	75.2	84.0	87.9	82.8	90.9	97.1
Y	4.9	6.5	11.2	5.8	3.1	9.4	6.6	12.9	10.0	11.0	11.9
Zr	2.5	2.4	3.9	3.2	1.2	3.4	3.1	6.3	4.1	7.2	12.5
La	0.6	1.2	2.1	0.6	0.3	0.9	0.8	1.1	1.0	1.6	2.0
Ce	2.6	3.4	5.5	3.4	1.4	4.3	3.5	5.6	4.3	5.7	7.0
Nd	---	---	---	---	1.8	5.1	3.9	7.0	5.4	6.0	7.0
Sm	1.5	1.6	1.4	3.8	0.7	1.9	1.3	2.8	2.3	2.2	2.6
Eu	---	---	---	---	0.2	0.4	0.4	0.7	0.5	0.5	0.6
Yb	---	---	---	---	0.2	0.9	0.5	1.1	0.9	1.0	1.1
Lu	---	---	---	---	0.0	0.1	0.1	0.2	0.1	0.2	0.2
Hf	---	---	---	---	0.1	0.2	0.2	0.3	0.2	0.3	0.5

<i>high-Zr cpx</i>											
	cpx-c	cpx-g	cpx-j	cpx-k	cpx-p	cpx-q	cpx-r	cpx-s	cpx-t	cpx-u	cpx-v
Sr	73.2	102.7	98.2	97.2	102.4	100.3	114.0	108.1	91.0	100.7	103.1
Y	20.6	41.9	31.3	29.2	39.1	30.8	24.0	27.7	25.5	29.6	36.9
Zr	24.0	64.5	35.3	32.9	56.5	38.6	22.2	40.2	24.9	34.5	46.2
La	4.6	6.4	3.1	2.9	4.3	3.7	2.9	4.5	3.5	3.4	4.2
Ce	15.0	24.0	14.2	12.9	19.4	16.3	12.4	17.7	14.2	16.3	16.9
Nd	---	25.5	16.8	15.6	20.8	17.9	13.0	17.2	14.0	16.7	20.8
Sm	5.9	8.3	5.9	5.5	6.8	6.7	4.0	5.2	3.8	5.4	5.9
Eu	---	1.9	1.2	1.1	1.7	1.2	1.0	1.4	1.1	1.1	1.5
Yb	---	3.7	3.1	2.8	3.3	3.0	2.4	3.3	2.6	2.8	3.6
Lu	---	0.7	0.5	0.4	0.7	0.5	0.4	0.5	0.5	0.5	0.7
Hf	---	2.8	1.5	1.6	2.2	1.6	1.1	1.9	1.1	1.6	2.0

Trace element data collected using the Element I high-resolution ICP-MS with New Wave UP213 laser ablation system at Pennsylvania State University

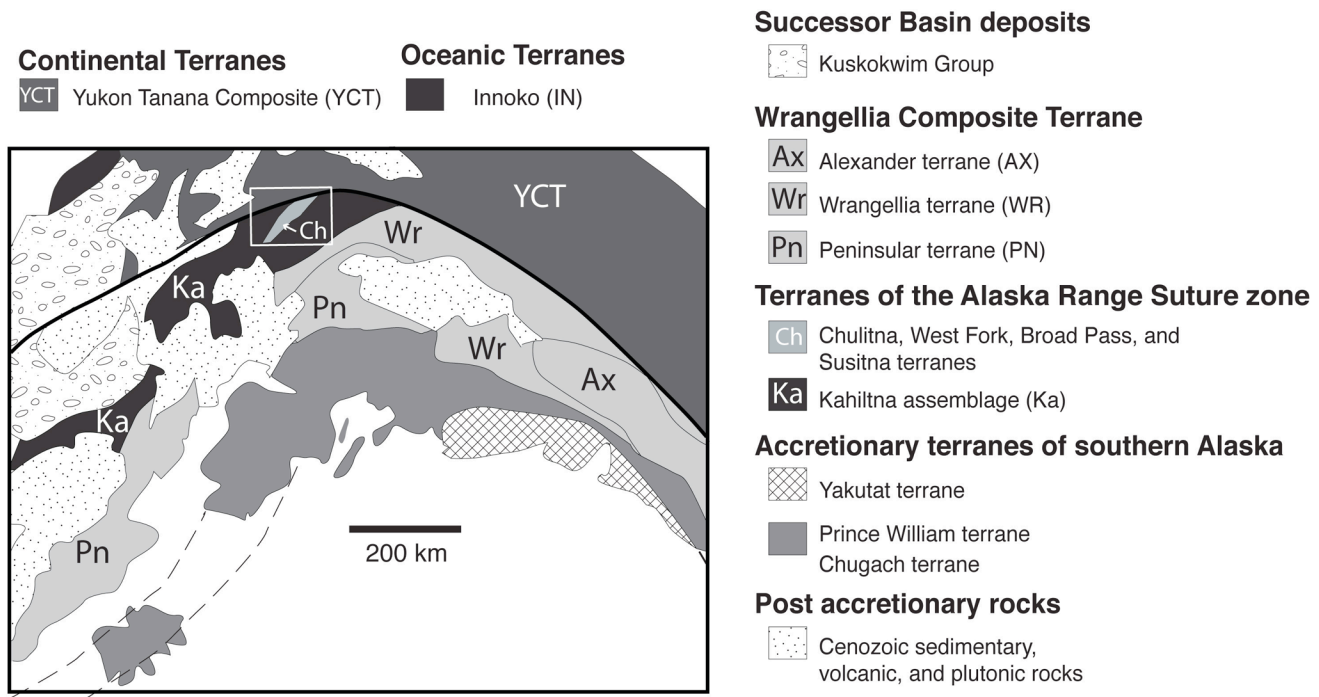


Figure 1

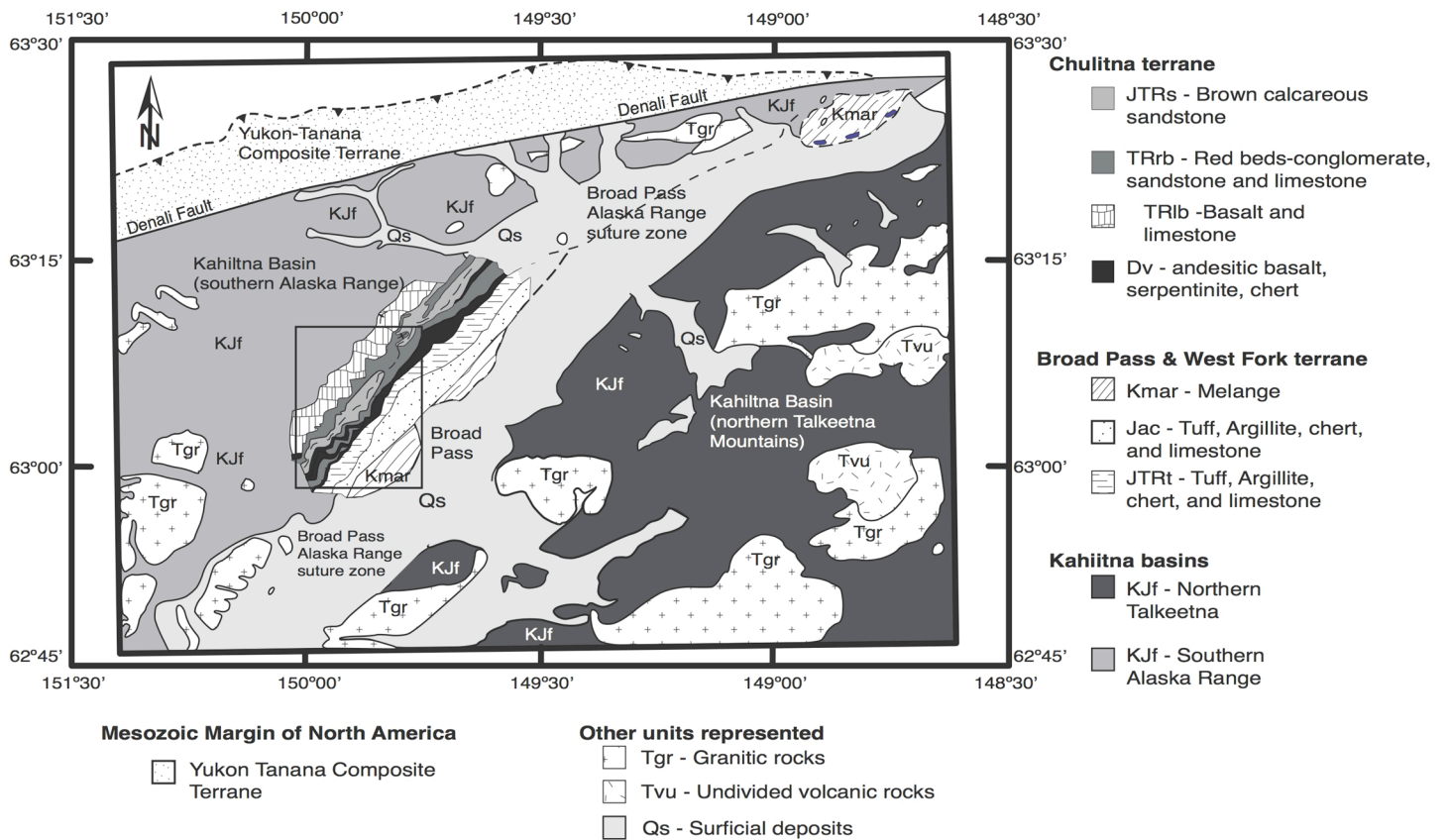
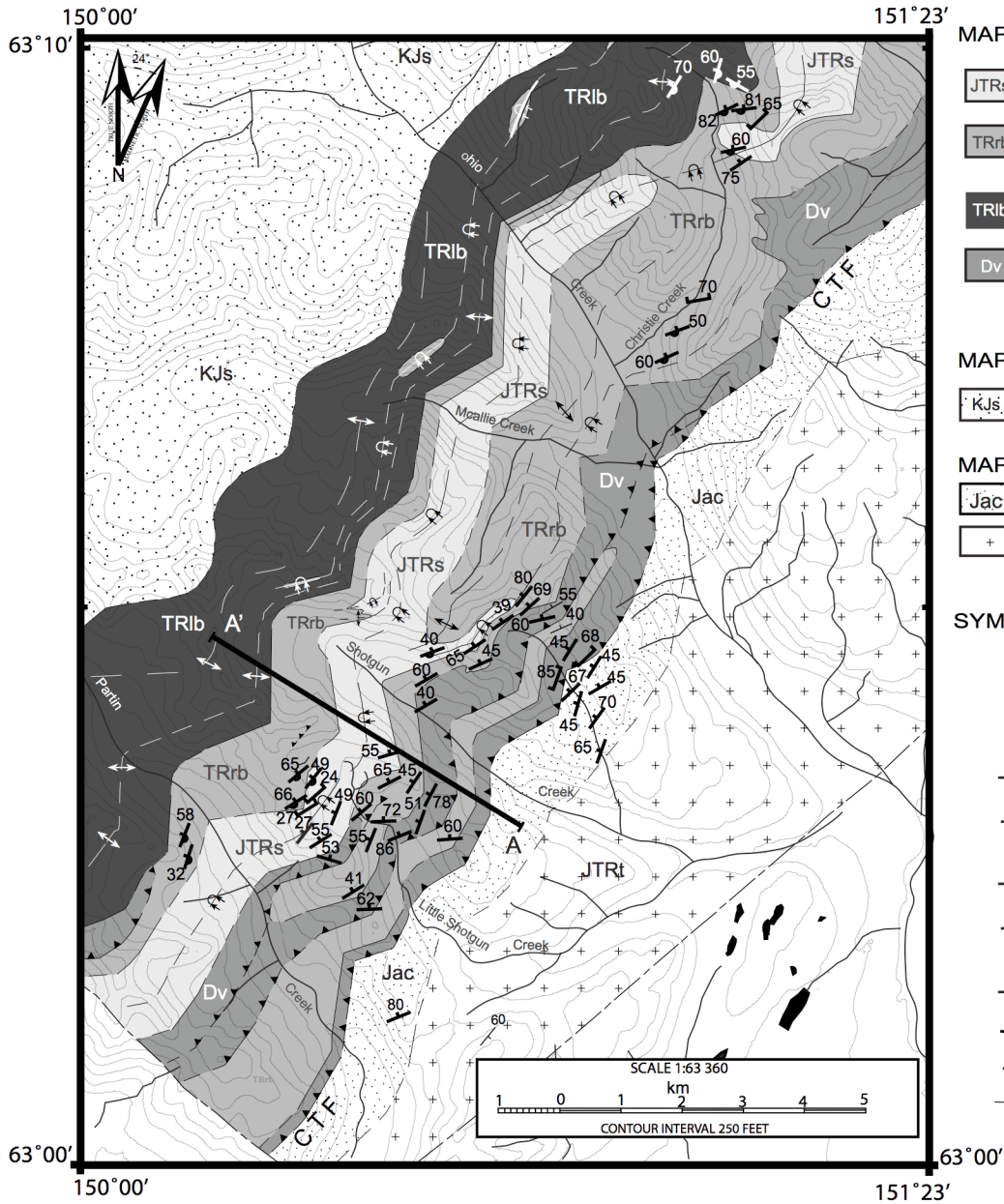


Figure 2



### MAP UNITS CHULITNA TERRANE

- JTRs** JTRs - Sandstone and calcareous sandstone with lenses of impure limestone
- TRrb** TRrb- Red-colored sedimentary breccia, conglomerate, sandstone, and siltstone with limestone
- TRib** TRib - Basalt (pillowed, columnar, massive, and brecciated) intercalated with limestone.
- Dv** Dv- Volcanics, Vesicular basalt to basaltic andesite, basaltic breccia, serpentinite and minor red radiolarian chert.

### MAP UNITS SOUTHERN ALASKA RANGE BASIN

- KJs** KJs - Sandstone, argillite, and chert

### MAP UNITS WEST FORK TERRANE

- Jac** Jac- Argillite and chert with minor tuff
- +** JTRt - Massive Tuff

### SYMBOLS

- 70  
Strike and Dip of beds
- Cleavage
- Overturned syncline observed fold axis
- Overturned syncline interpreted fold axis, arrows point towards directions of dip
- Anticline observed fold axis
- Anticline interpreted fold axis
- Interpreted contact
- Observed contact
- Thrust fault interpreted
- Thrust fault observed
- Contact

Figure 3

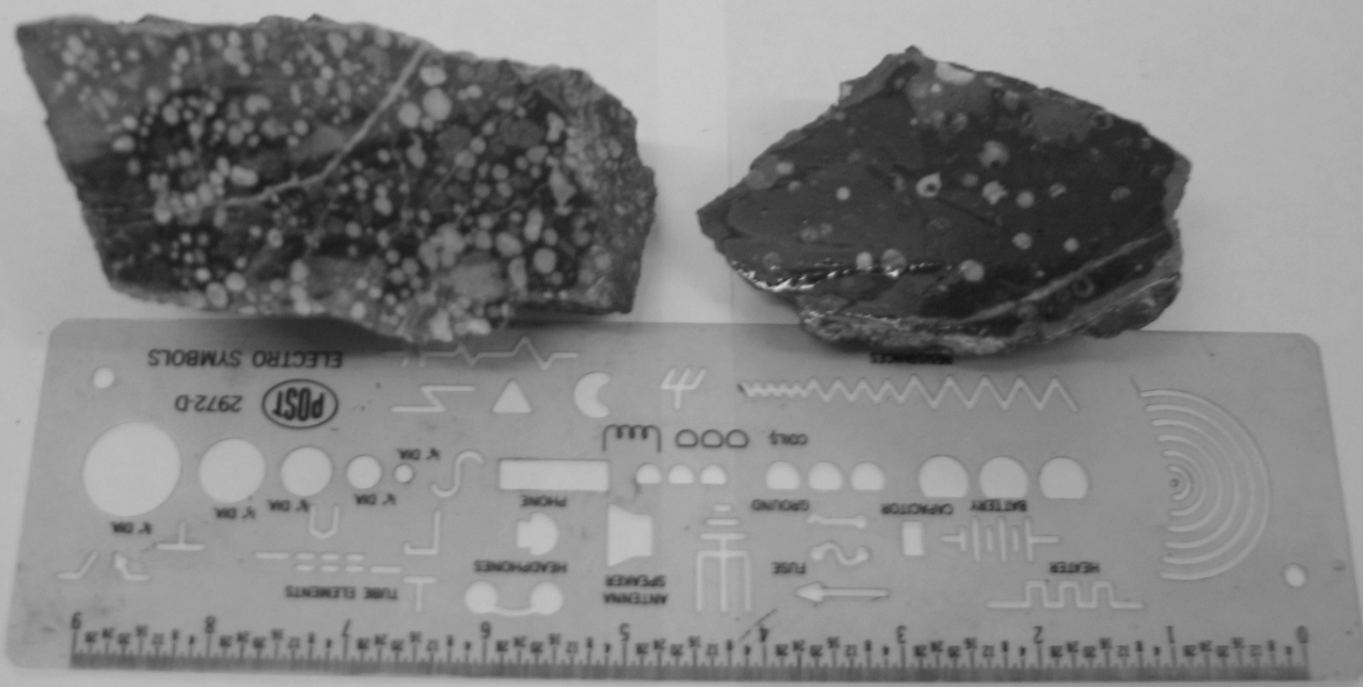


Figure 4

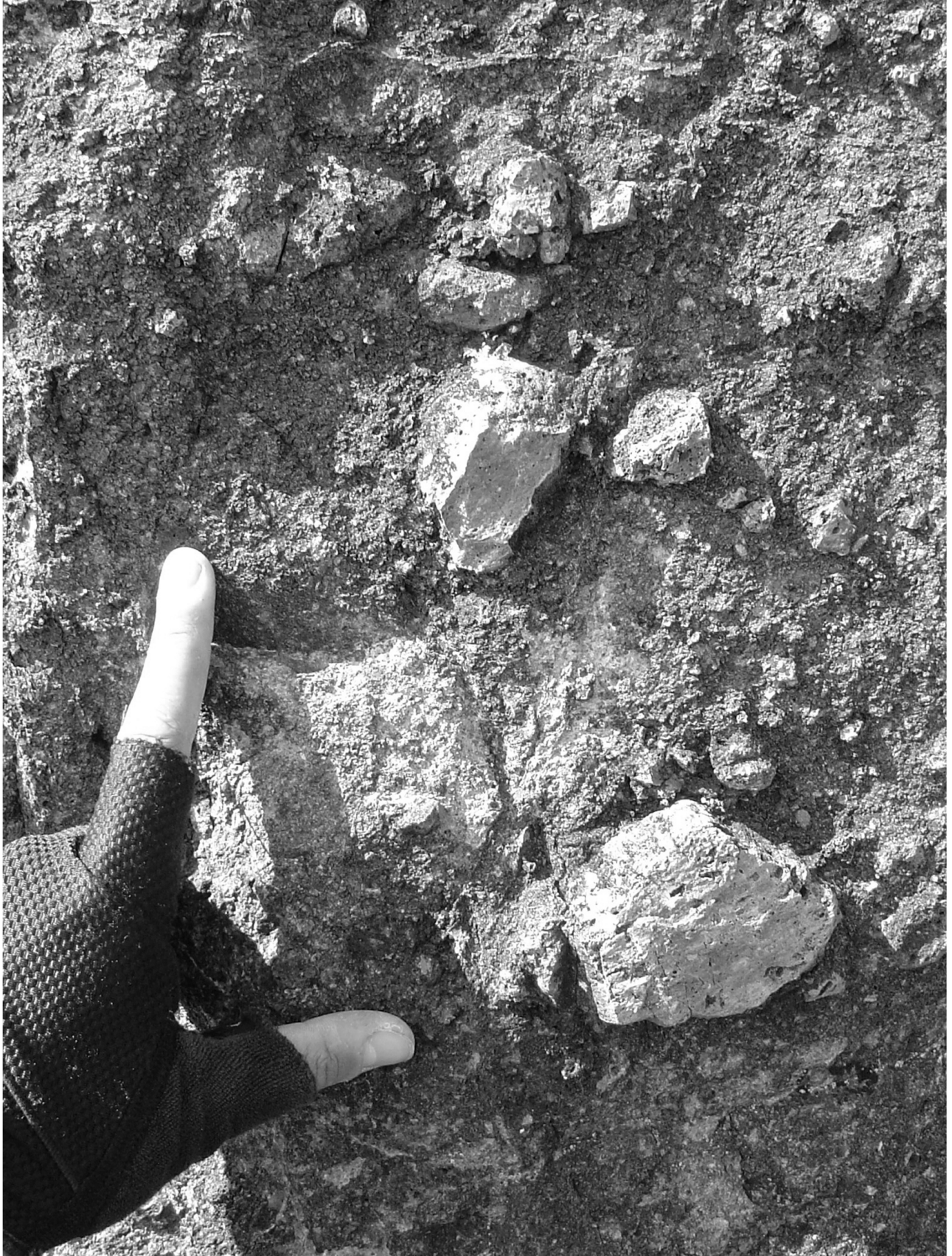


Figure 5



Figure 6a

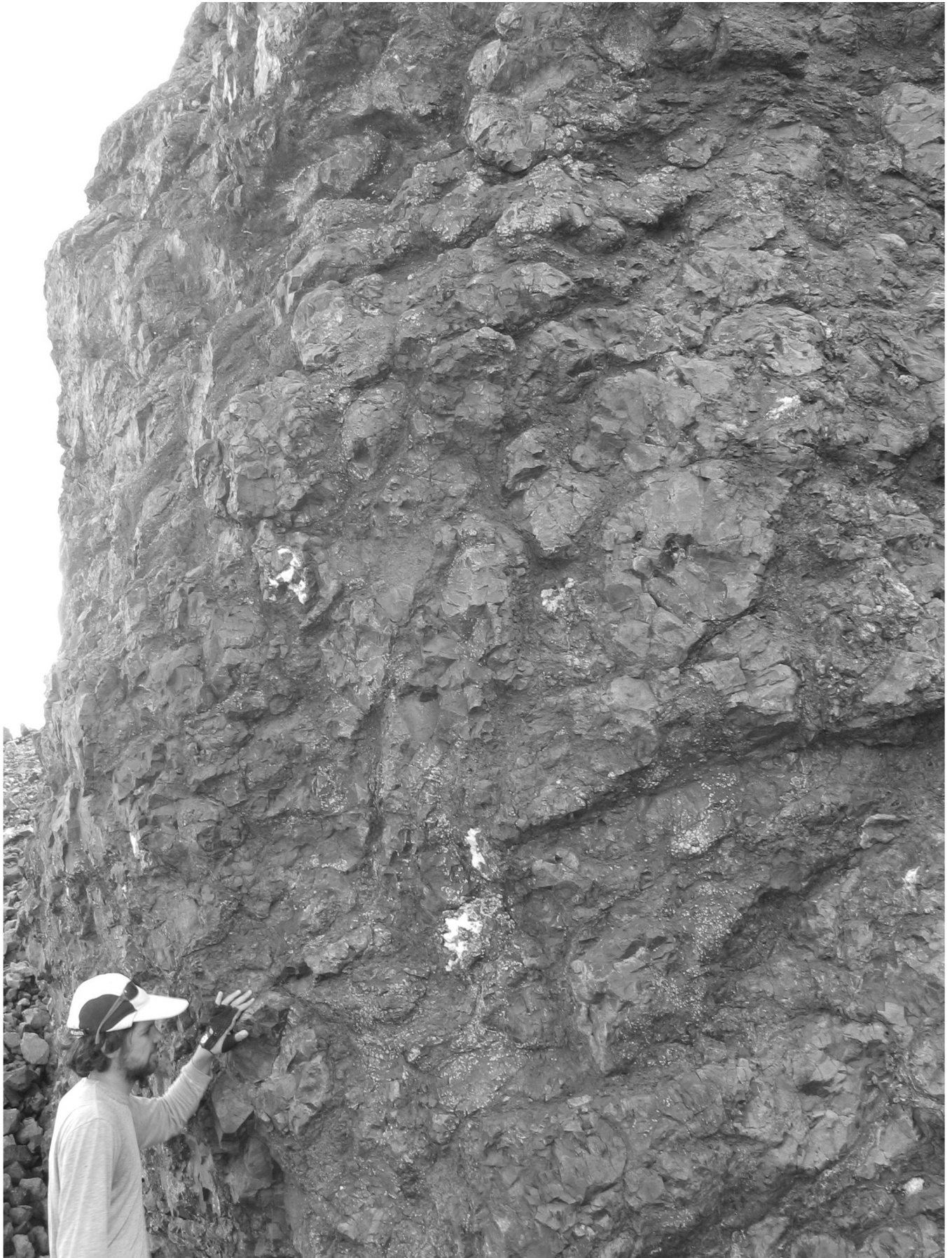


Figure 6b

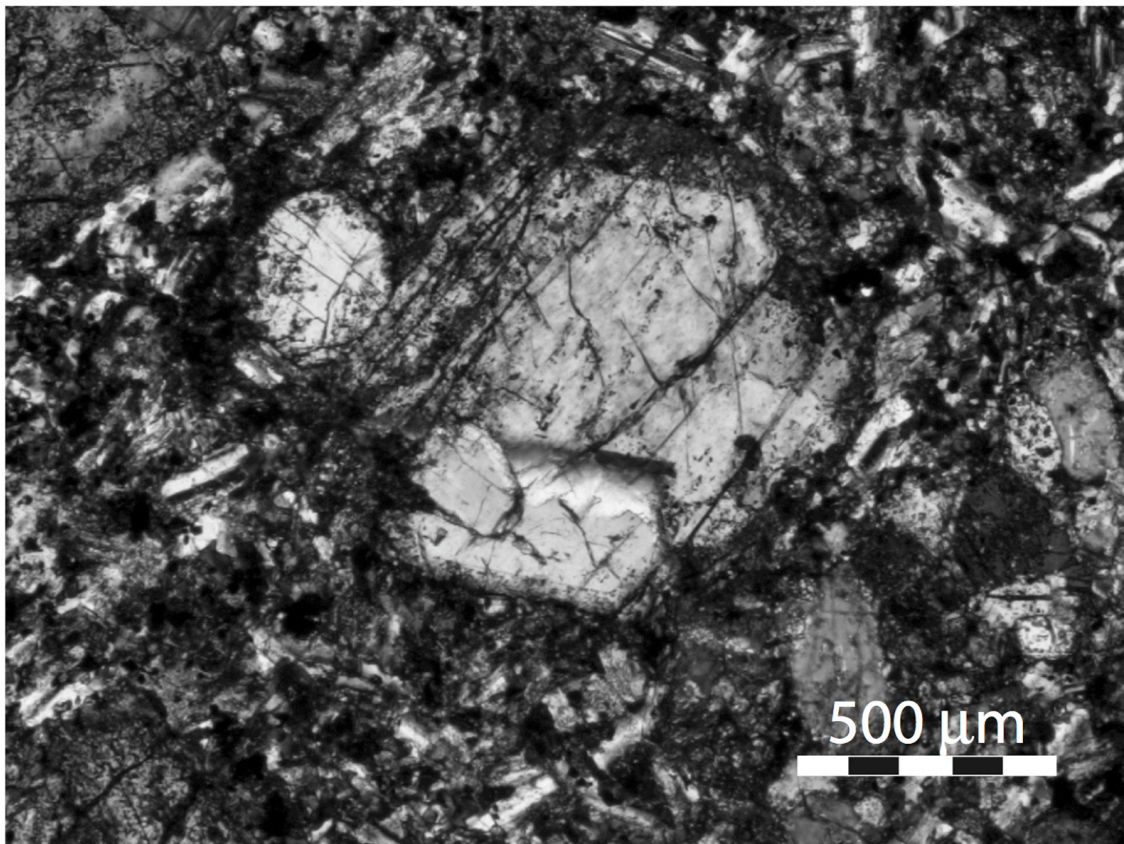


Figure 7

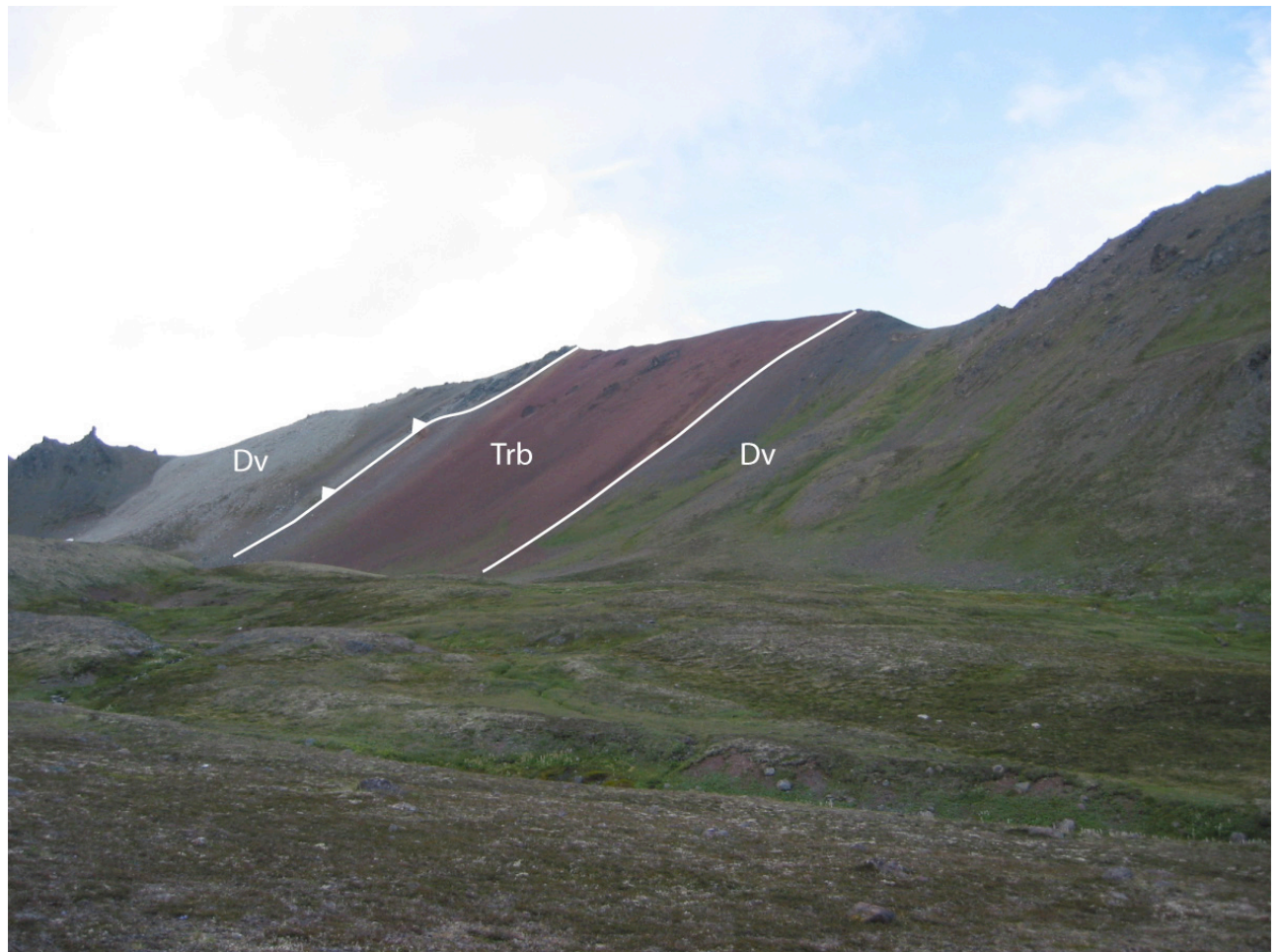


Figure 8a



Figure 8b



Figure 9

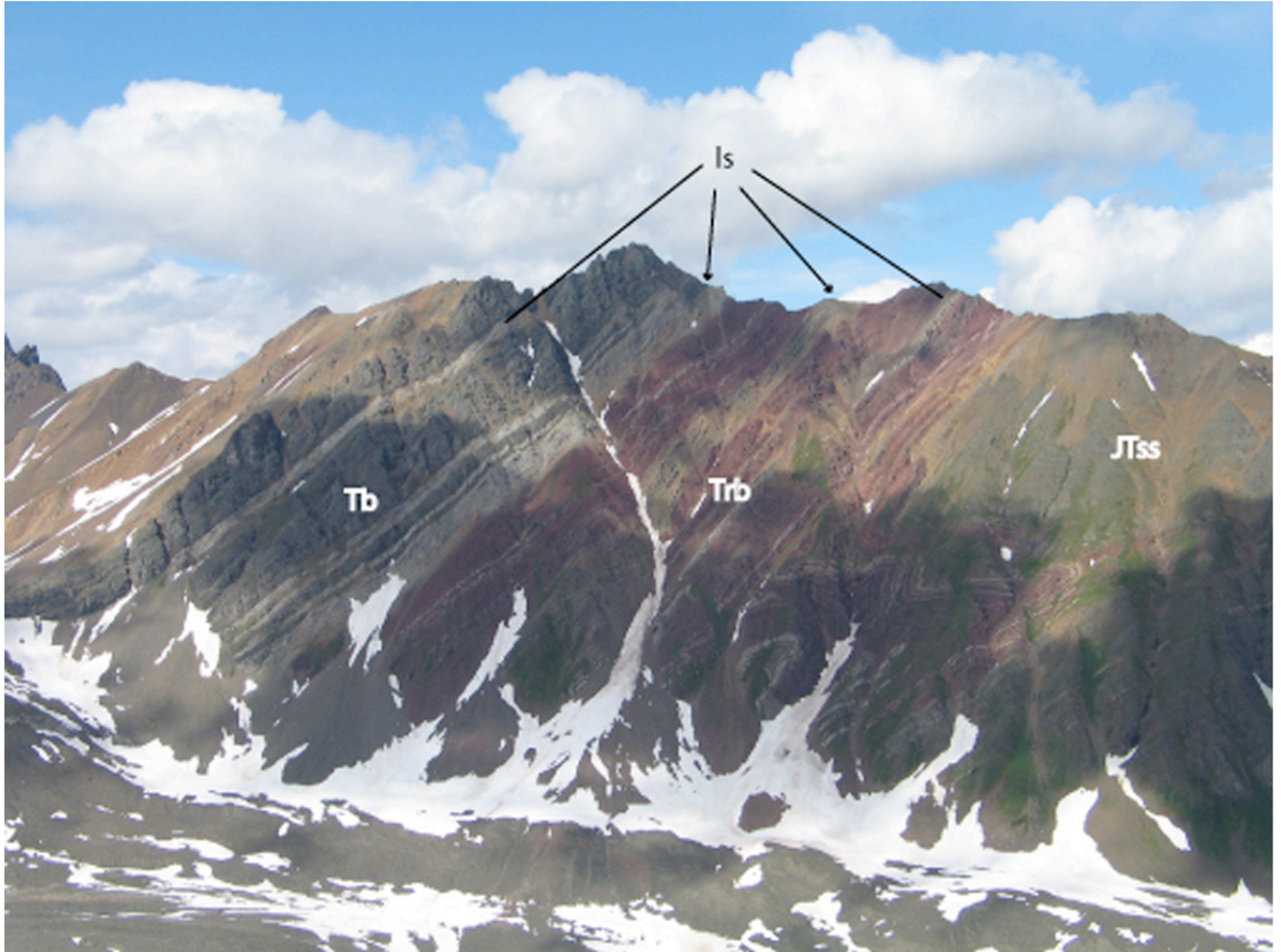


Figure 10

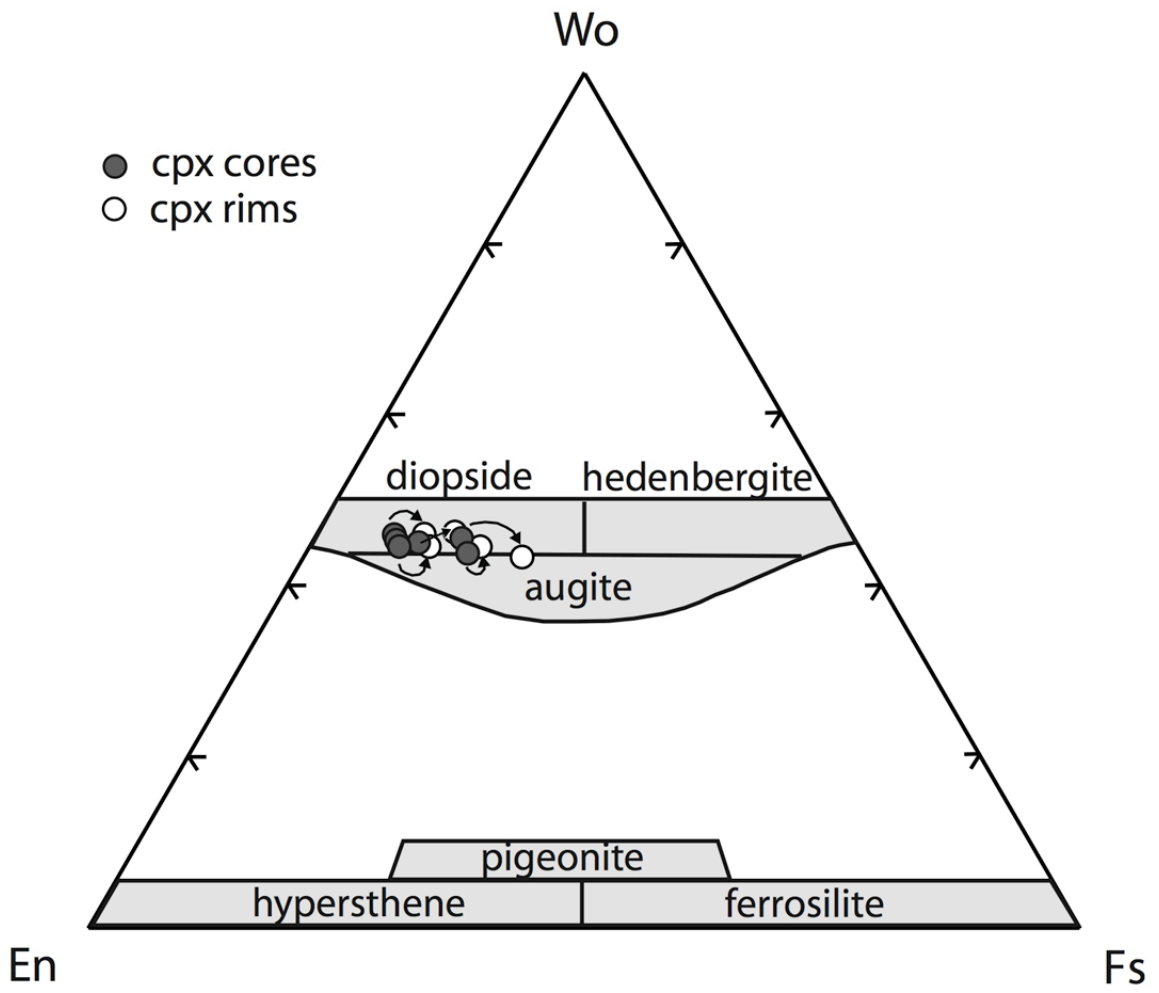


Figure 11

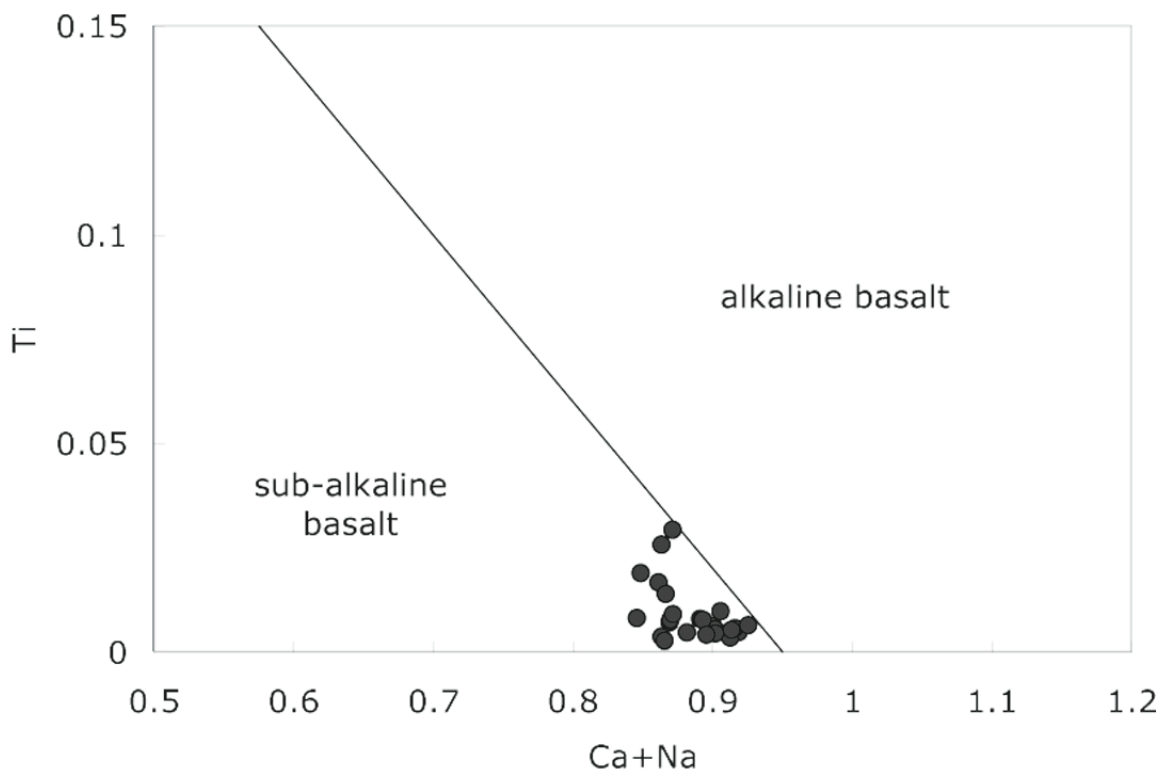


Figure 12a

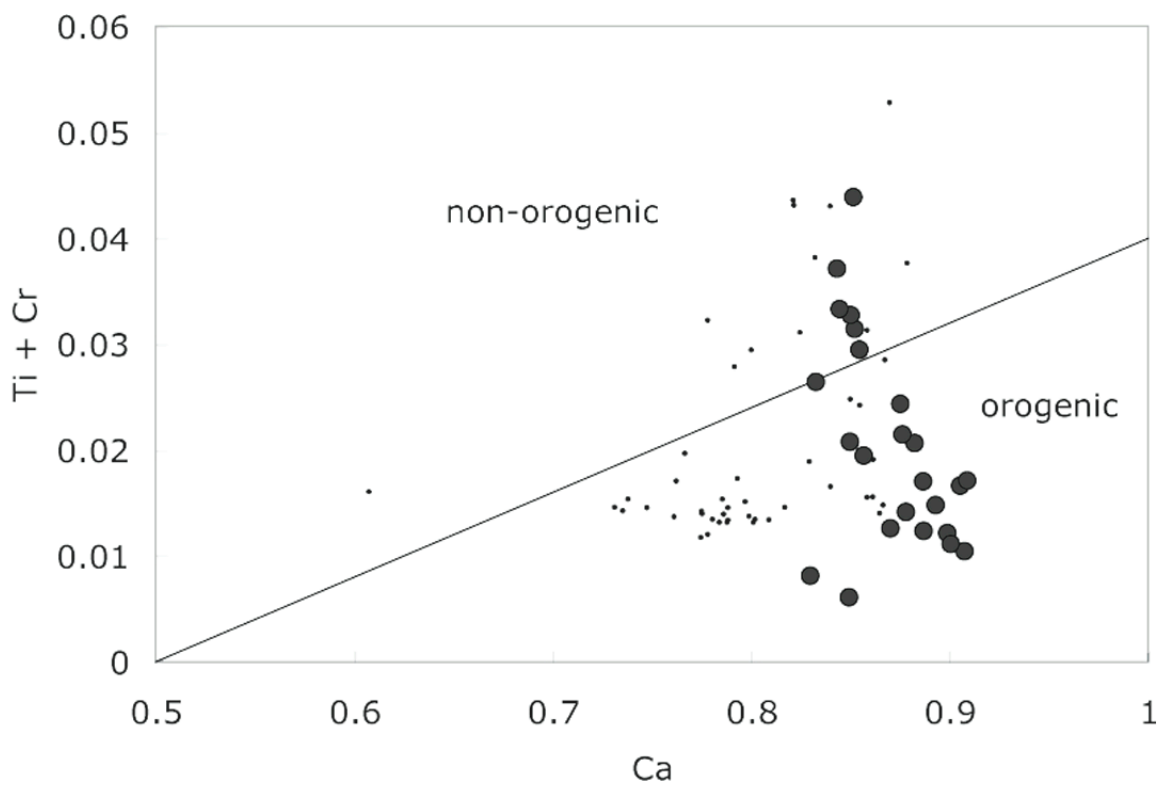


Figure 12b

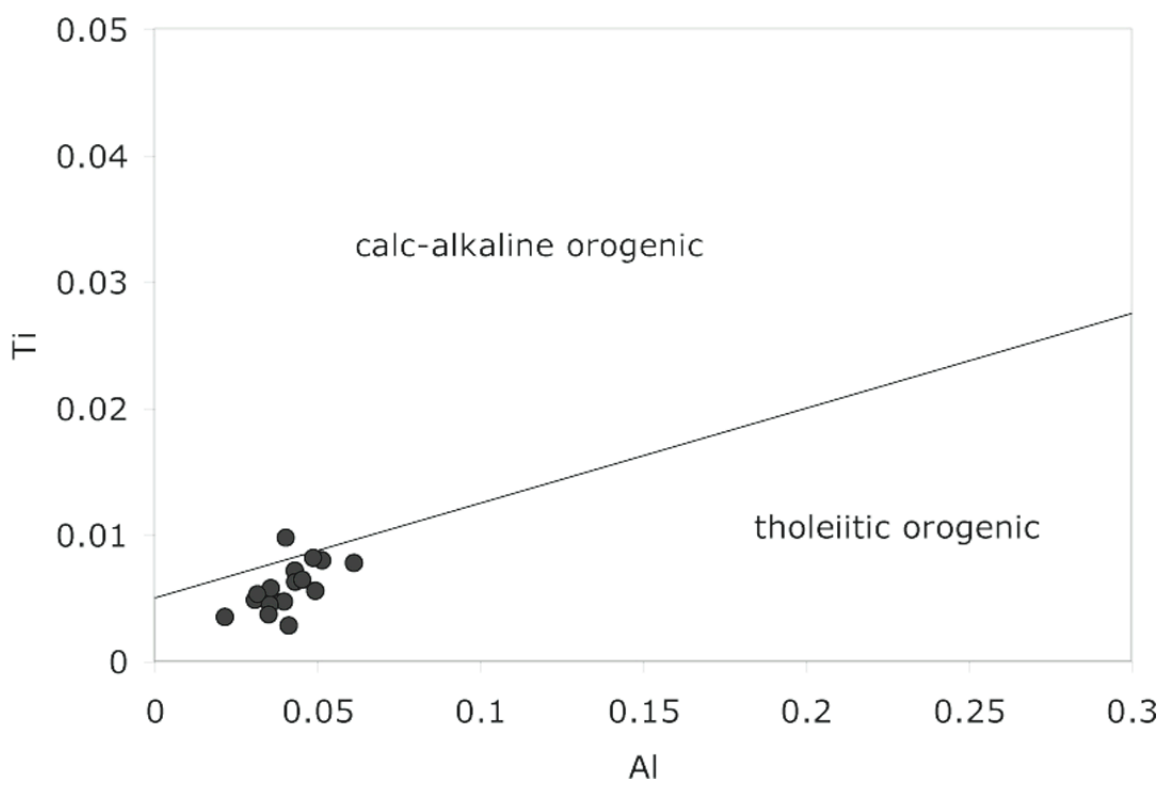


Figure 12c

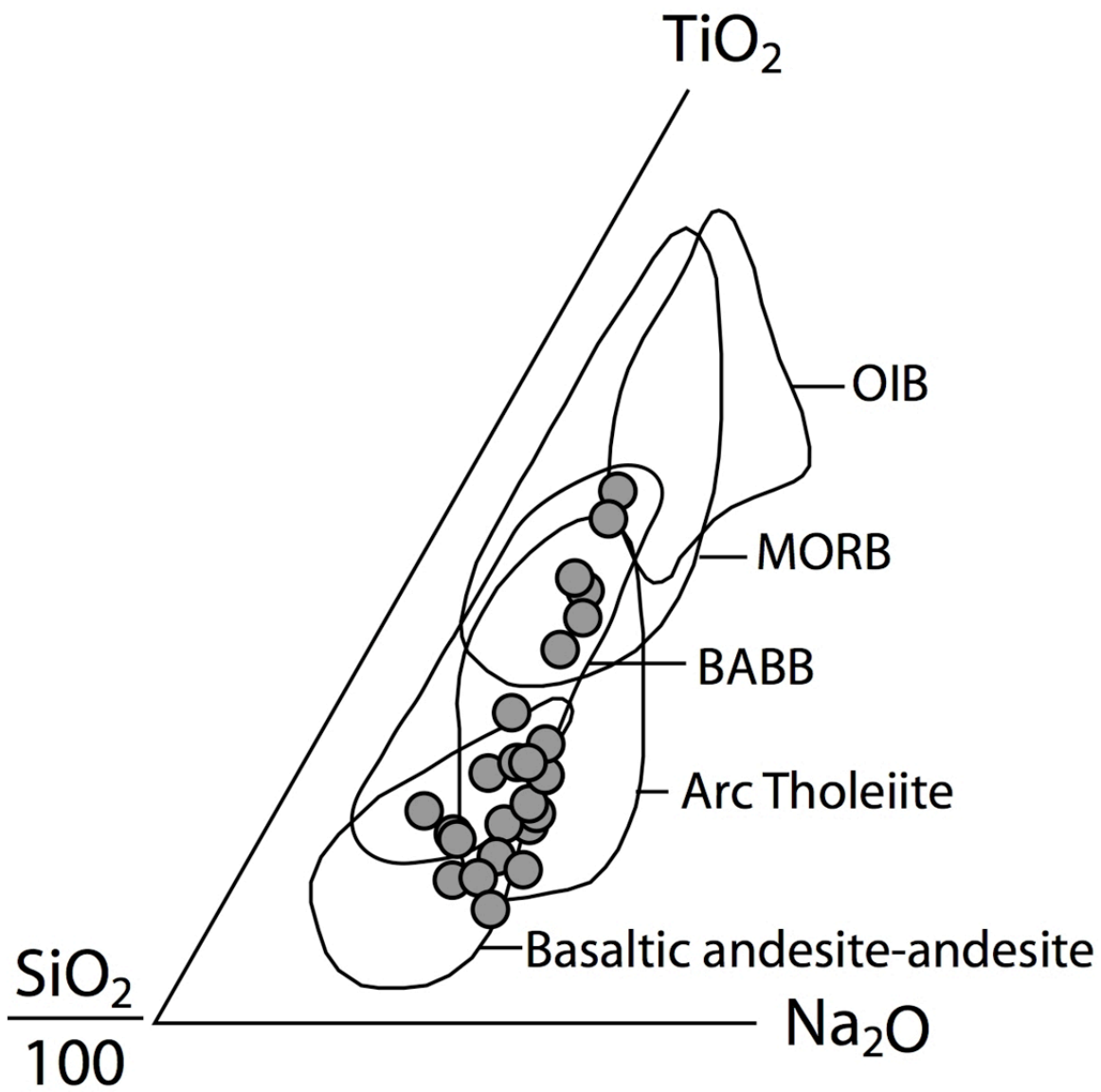


Figure 13

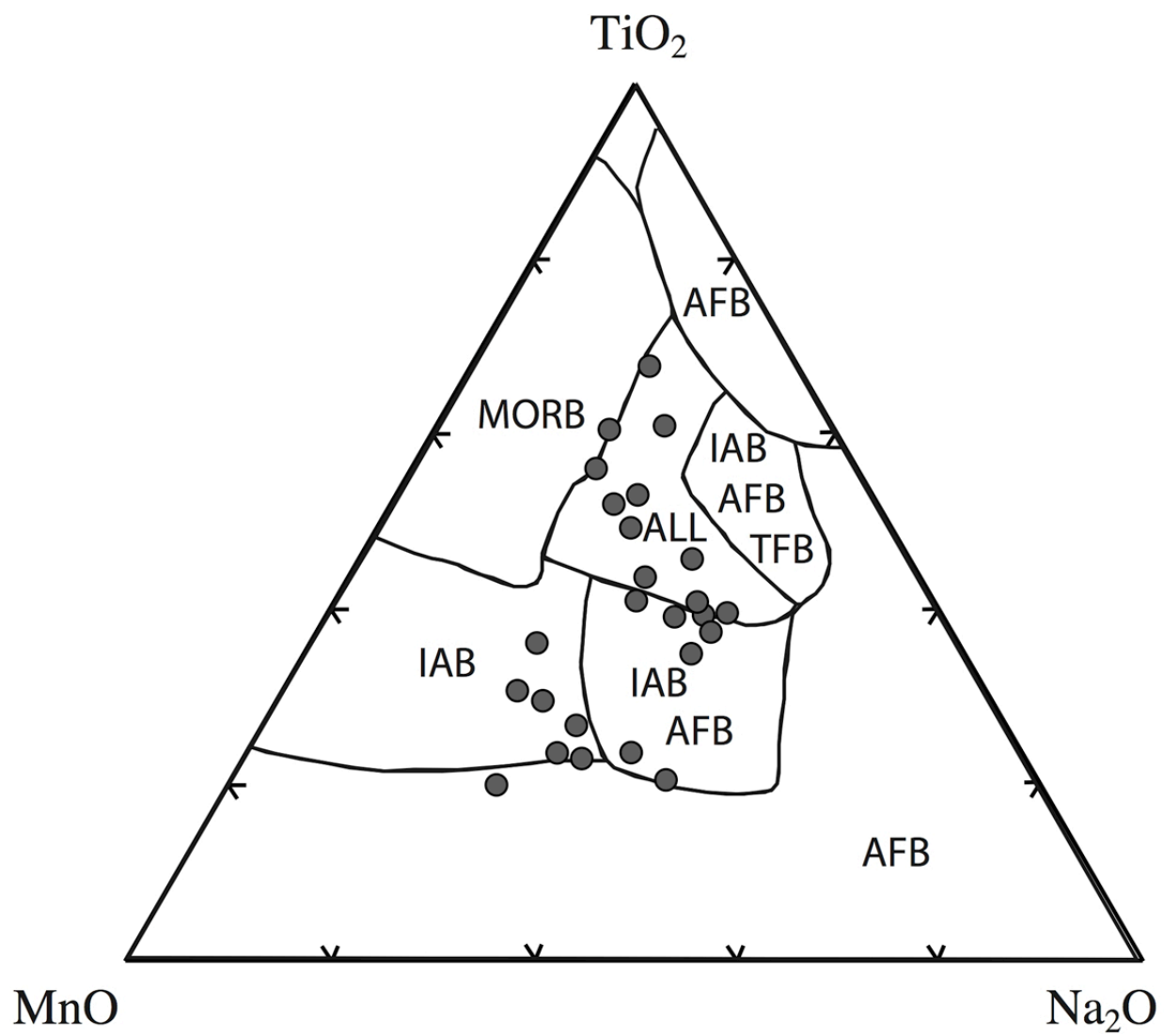


Figure 14

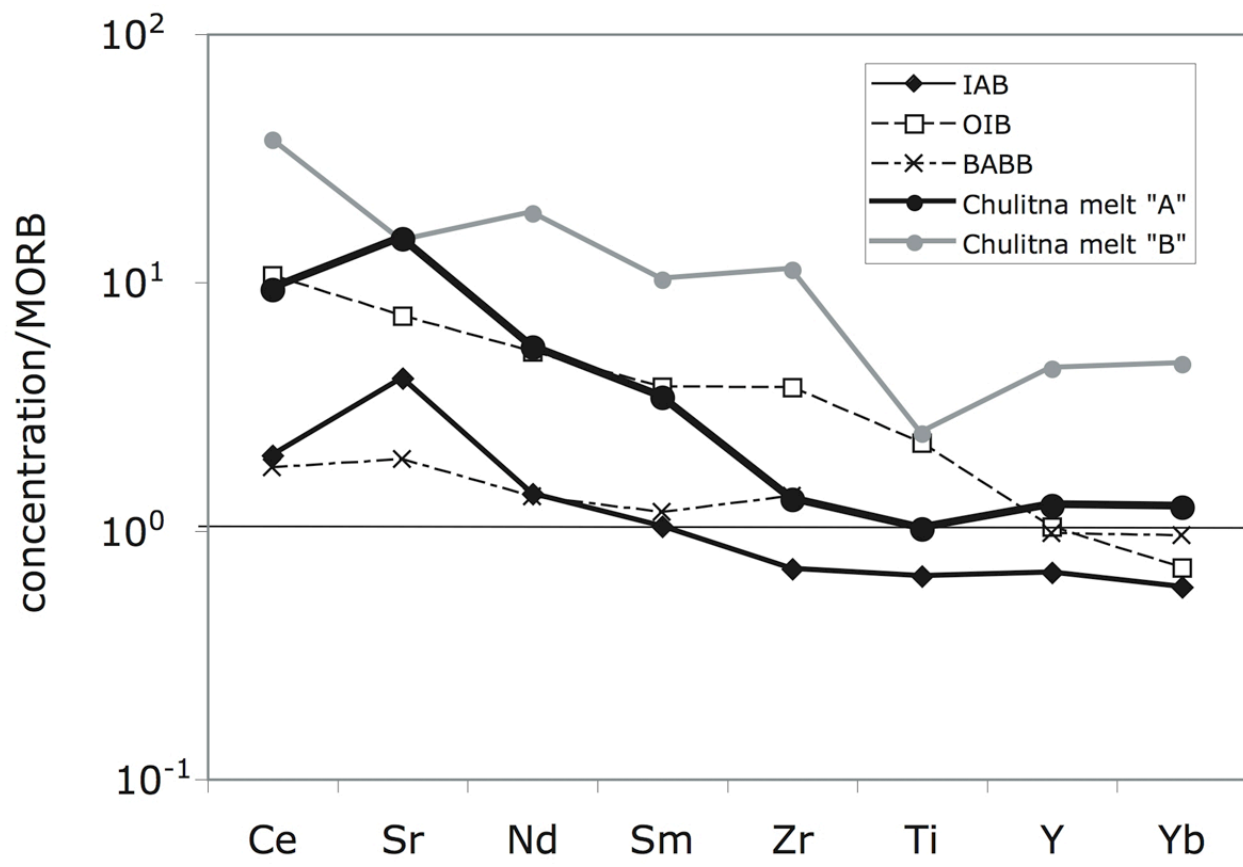


Figure 15

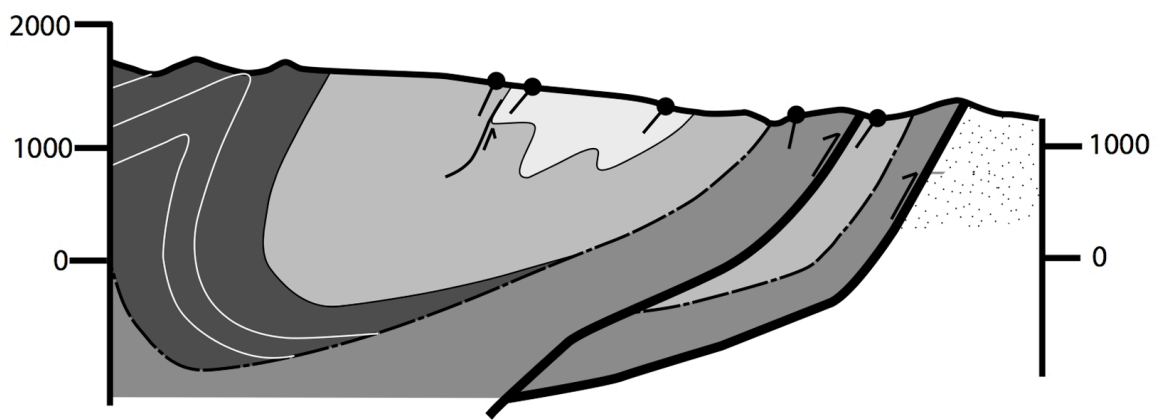


Figure 16a

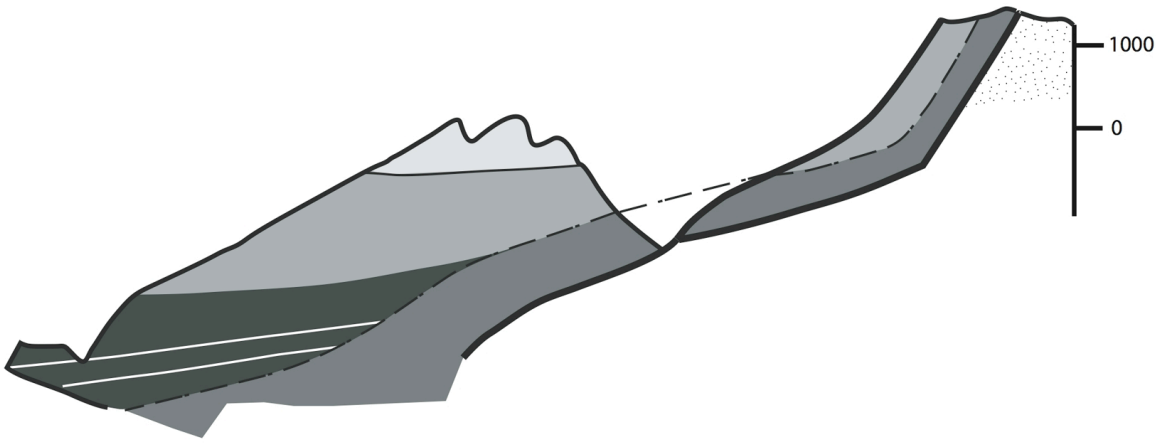


Figure 16b